AD-A147 256 HIGH MARANGONINUMBER CONVECTION IN A SQUARE CAVITY(U) 1/1
STANFORD UNIV CA CENTER FOR LARGE SCALE SCIENTIFIC
COMPUTATION A ZEBIB ET AL. 31 MAY 84 CLASSIC-84-06
UNCLASSIFIED N00014-82-K-0335 F/G 20/13 NL

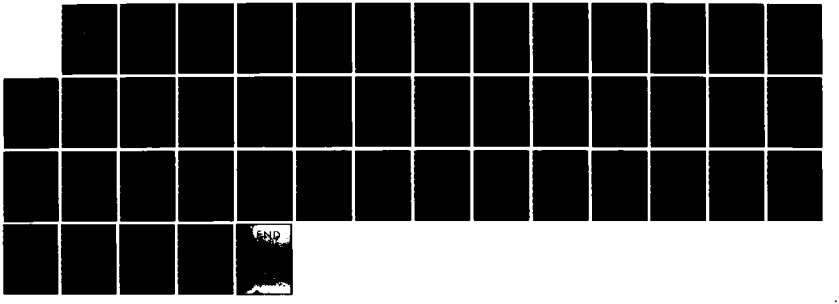

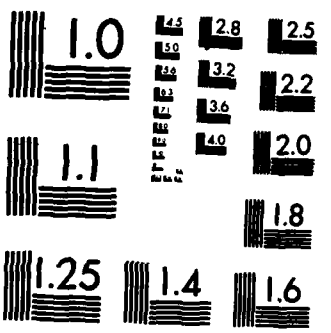
1.0
1.1
1.25
1.4
1.6
1.8
2.0
2.2
2.5
2.8
3.2
3.6
4.0
4.5
5.0

CLaSSiC Project
Manuscript CLaSSiC-84-06

July 1984

High Marangoni Number Convection in a Square Cavity

by

A. Zebib

G. M. Homsy

E. Meiburg

Center for Large Scale Scientific Computation
Building 460, Room 304
Stanford University
Stanford, California 94305

High Marangoni number convection in a square cavity

A. Zebib

Department of Mechanical and Aerospace Engineering

Rutgers University

New Brunswick, NJ 08903

G. M. Homsy

Department of Chemical Engineering

Stanford University

Stanford, CA 94305

&

E. Meiburg

DFVLR

Göttingen, West Germany

31 May 1984

ABSTRACT

We consider the steady thermocapillary motion in a square cavity with a top free surface in the absence of gravitational forces. The cavity is heated from the side with the vertical boundaries isothermal while the horizontal boundaries are adiabatic. The relative change in the surface tension is very small, i.e. an appropriate capillary number tends to zero, so that the free surface is assumed to remain flat at leading order. A finite difference method is employed to compute the flow field. Numerically accurate solutions are obtained for a range of Prandtl numbers and for Reynolds numbers as high as 5×10^4. Surface deflections are computed as a domain perturbation for small capillary number. In addition, asymptotic methods are used to infer the boundary layer structure in the cavity, in the limit of large values of the Reynolds number Re and the Marangoni number Ma. For a fixed Prandtl number Pr, it is shown that the Nusselt number, liquid circulation and maximum vorticity are asymptotic to $Re^{1/3}$, $Re^{-1/3}$ and $Re^{2/3}$, respectively. These results are in agreement with the computed solutions. The leading order solution for the free surface deformation is sensitive to the value of Pr. With $Pr > 1$, the depression near the hot corner may exceed the elevation near the cold corner. While a secondary elevation may be induced near the hot corner when $Pr < 1$.

A-1

1. Introduction

Convective motions driven by a temperature gradient along the interface between two immiscible fluids, due to the variation of surface tension with temperature, are of considerable interest and play an important role in small scale and/or low gravity hydrodynamics (Schwabe, 1981 and Ostrach, 1982). Because these thermocapillary flows occur in crystal growth melts and dominate the convective flows in the microgravity environment of space, there have been a number of recent studies of simplified two-dimensional models with negligible gravitational effects.

Sen & Davis (1982) consider steady thermocapillary convection in a differentially heated rectangular slot with a top free-surface. They present results valid for vanishingly small aspect ratio A (height/width) with the Reynolds number Re $\sim$ O(A), the Marangoni number Ma $\sim$ O(A) and the capillary number Ca $\sim$ O(A^4). The same problem is also studied by Strani, Piva & Graziani (1983) for A $\rightarrow$ 0 with Ca $\sim$ O(A^4) but with milder restrictions on Re and Ma. These studies are instructive in giving the flow field and surface deflection in a conduction-dominated regime, but give little information about strongly convective flows.

Strani et. al. (1983) also compute the thermocapillary motions in a rectangular cavity with A = 0.2, 1 and 5 and with the Prandtl number Pr = 1 (i.e. Ma = Re). They allow for free-surface deformation and conclude, as expected, that for Ca = 0.1 surface deformation have a negligible influence on the flow field. Because they use a coarse mesh for their finite-difference computations, their results are accurate only for low Re and Ma. Since vigorous motion occurs in float-zones at high values of Ma and Re (Schwabe 1981, Ostrach 1982), there is a need for further study of this model problem. Axisymmetric modeling of a half-floating zone configuration has been considered by Fu & Ostrach (1983) where they compute the flow field at different values of Re, Ma and Pr. Many of the features of their solutions are common to ours.

The stability of such flows is of great interest. As the experiments of Preisser, Schwabe & Scharmann (1983) and Kamotani, Ostrach & Vargas (1983) have shown, steady convection is stable

only below certain values of the Marangoni number. Above the critical values, the flow is typically an oscillatory one, with commensurate changes in the transport properties and important implications in material processing applications. The only stability analysis of this class of flows is that of Smith & Davis (1983a,b) who restricted their attention to plane-parallel flow profiles appropriate to conduction-dominated situations. It is not known how relevant the stability limits calculated by these authors are to strongly convective situations.

In this paper we compute steady thermocapillary flows in a square cavity (A = 1) by a finite-difference procedure. O r objective is to obtain accurate numerical solutions to the stated problem at as a high Reynolds number as possible, in order to characterize the nature of strongly convective flows of this general class. Only the case Ca $\rightarrow$ 0 is considered, so that the free-surface is assumed flat at a leading order. Surface deflections are computed by domain perturbation. Boundary layer formation at different values of Pr is observed at large values of Ma and Re. We use the numerical results to infer the relevant scalings of a consistent boundary layer picture of the flow, valid asymptotically as Re $\rightarrow \infty$. We do not attempt to present a complete boundary layer theory since solving the boundary layer problem seems to be as difficult as solving the full equations of motion.

2. Mathematical model

The physical model consists of a rectangular cavity of average height d and width w containing an incompressible, Newtonian liquid. The top horizontal boundary is a free surface open to a passive gas. The vertical rigid, isothermal walls are differentially heated and are kept at temperatures $\pm T_0/2$ relative to an arbitrary reference temperature. The bottom boundary is rigid and adiabatic. In the absence of gravity, the nondimensional equations for the liquid motion are (Sen & Davis 1982)

$$\nabla.\underline{V} = 0 \quad , \tag{2.1}$$

$$Re\nabla.(\underline{V}\underline{V}) = -\nabla p + \nabla^2\underline{V} \quad , \tag{2.2}$$

$$Ma\nabla.(\underline{V}T) = \nabla^2 T \quad , \tag{2.3}$$

Here length, velocity, temperature and pressure are dimensionless with respect to d, $\gamma T_0/\mu$, T_0 and $\gamma T_0/d$, respectively, where μ is the viscosity and surface tension is assumed to decrease with temperature increase at a constant rate γ. The Reynolds number and the Marangoni numbers are defined in the usual way by

$$Re = \gamma T_0 d/(\mu\nu) \quad , \tag{2.4}$$

$$Ma = Re\ Pr \quad , \tag{2.5}$$

where ν is the kinematic viscosity and the Prandtl number $Pr = \nu / \kappa$, and κ is the thermal diffusivity.

The motion is referred to a Cartesian coordinate system with the origin at the middle of the bottom boundary with the y axis parallel to the side walls. The boundary conditions on the fixed surfaces are:

$$\underline{V}(\pm 1/(2A), y) = 0 \quad ; \quad \underline{V}(x,0) = 0 \quad , \tag{2.6a,b}$$

$$T(\pm 1/(2A), y) = \mp 1/2 \quad ; \quad T_y(x,0) = 0 \quad , \tag{2.7a,b}$$

where subscripts denote partial differentiation and the aspect ratio A = d / w which we set to unity in the remainder of this paper. The x and y components of $\underline{V}$ will be denoted as usual by u and v, respectively.

In addition to Re, Ma and Pr, there is an additional dimensionless parameter which is a measure of

the free surface deformation. This is the capillary number Ca and is given by

$$Ca = \gamma T_0/\sigma_0 \quad . \tag{2.8}$$

where σ_0 is an average value for the surface tension. We see that $Ca \sim \Delta\sigma/\sigma_0$, and in experiments is generally a small quantity; Kamotani et. al. (1983). We thus consider the case $Ca \to 0$, i.e. only small variations in σ and in surface deformation are allowed. If in addition to small Ca, we assume the contact angle is $\pi/2$, the surface is initially located at a height $y = 1$. Thus to leading order in Ca, we assume a flat free surface with the boundary conditions

$$u_y(x,1) = -T_x(x,1) \quad ; \quad T_y(x,1) = 0 \quad . \tag{2.9a,b}$$

Corrections to the surface are computed as follows. If we denote the departure of the free surface from $y = 1$ by $h(x)$, then in the limit $Ca \to 0$ we find

$$h_{xx} = -Ca\ p \quad ; \quad h(\pm 1/2) = 0 \quad . \tag{2.10a,b}$$

Equation (2.10b) assumes a fixed contact line. Other boundary conditions are possible; Sen & Davis (1982). Because the pressure field $p(x,y)$ is determined only to an additive constant, an additional constraint on $h(x)$ from global continuity is

$$\int_{-1/2}^{1/2} h\ dx = 0 \quad . \tag{2.11}$$

Thus $h(x)$ can be determined to $O(Ca^2)$ by solving (2.10-2.11) once p has been found. We note for future reference that the surface vorticity $\omega_s = -u_y(x,1)$ is simply the surface temperature gradient.

3. Numerical procedure

Solutions to the system of equations (2.1), (2.2), (2.3), (2.6), (2.7) and (2.9) must be constructed by some numerical method. At a first glance it would seem that a spectral method with an infinite order convergence (Gottlieb & Orszag 1977) may be suited to the problem. However, the hot and cold corners on y = 1 are singular. The vorticity

$$\omega = v_x - u_y \quad , \tag{3.1}$$

is discontinuous at these corners, and will assume different values as a corner is approached on different paths. Indeed, following the analysis of Moffatt (1964) it can be shown that, in the vicinity of the hot corner, the vorticity is given by

$$\omega = -T_x(-1/2,1)\ (1-4\theta/\pi), \tag{3.2}$$

where the angle θ is 0 on x = -1/2 and $\pi/2$ on y = 1. It should be noted that the flow field corresponding to (3.2) is valid only very close to the corner so that the flow is locally a Stokes flow. A similar expression holds for ω near the cold corner. It is thus expected that ω will vanish on the diagonals as the corners are approached.

Since this discontinuity will limit the convergence of any spectral method we opt for a finite difference approach. The method and the iteration procedure we use to solve the finite difference equations are described in detail by Patankar (1981). Briefly, the computational region is divided into rectangular control volumes with the grid points located at the geometric centers of these cells. Additional boundary grid points are included where the boundary conditions (2.6,7,9) are imposed. The finite difference equations are obtained by integrating the governing equations (2.1,2,3) over the control volumes with assumed local linear variations in any of the primitive variables. The convection and diffusion fluxes are approximated by a power-law scheme. The staggered location for the velocity components is adopted and the velocity-pressure coupling treatment follows Patankar's (1981) revised procedure. A line-by-line iteration to solve the discretized equations is used with one completed iteration comprising five double sweeps of the field. Under-relaxation in solving for u, v

and T was required; a relaxation factor of 0.85 was used throughout.

After a number of solutions were computed on uniform grids with 65 x 65 and 80 x 80 mesh points, we used a nonuniform grid with 62 points in the x direction and 54 points in the y direction, with the highest concentration of the mesh points near the cold corner where, as we shall see, the sharpest gradients occur. The smallest control volume at the cold corner is a square with side length 0.005. The rectangular cell at the hot corner has an x extent of 0.01. The mesh spacing was gradually increased away from the cold and hot corners in both the x and y directions. The largest mesh spacing near the middle of the bottom boundary is less than 0.05. All computations were performed on a VAX 11/780. A converged solution requires from 250 to 450 iterations, with each iteration completed in less than 25 CPU seconds. Convergence was assumed when the largest variation in any of u, v, p and T was less than some convergence tolerance which we set to 10^{-5}. For extreme values of Pr, we also performed some computations on a nonuniform mesh with the same smallest elements but with 70 x 60 mesh points.

In table I we list some representative computed results with different grids from which we claim accuracy within 3% for results with the 62 x 54 grid. It should be noted that the largest "error" is in the magnitude of of circulation $-\psi_{max}$ (here ψ is the streamfunction). This is especially true at large Re and when the point at which $-\psi_{max}$ occurs is located far from the top corners, i.e. where mesh spacing is relatively large. Because we use the conservative (divergence) form of the governing equations, an exact solution of the difference equations should result in equal values for the Nusselt numbers computed on the hot and cold boundaries Nu_- and Nu_+, respectively. Decreasing the convergence tolerance results in yet closer values for Nu_- and Nu_+ than those listed in table I.

4. Numerical results; Pr = 1

Our primary interest is in the character of the motion at large values of Ma and Re. Equation (2.3) shows that Ma measures the strength of temperature (thermal energy) convection to diffusion. Thus large values of Ma will lead to the formation of thermal boundary layers. Equations (2.1) and (2.2) can be reduced to the vorticity transport equation

$$Re\nabla.(\underline{V}\omega) = \nabla^2\omega \quad , \qquad (4.1)$$

and hence large Re implies the formation of regions of concentrated vorticity, in particular near the free surface. We first consider the case Pr = 1, i.e. simultaneous formation of both temperature and vorticity layers with Re = Ma.

With Pr = 1, we compute the thermocapillary motion for $10^2 \lesssim Re \lesssim 10^4$. As expected, the flow consists of a major closed circulation, accompanied by Moffatt corner eddies at the two lower corners. The temperature is distorted from a linear conductive field by this circulation, especially at high Ma. The surface temperature distribution is of key interest, since it is the gradient of this quantity which, through the thermocapillary stress, drives the motion. As an example of these features, we show in Figure 1a-c the streamlines, isotherms and iso-vorticity contours for Re = Ma = 10^3. As can be seen from Figure 1c, there is a large concentration of vorticity near the stagnation point near the cold (right) boundary. It is further seen that the stagnation point near the hot (left) boundary exhibits little, if, any, boundary layer behavior. The dividing $\omega = 0$ line is oriented at 45°, as required by (3.2).

In Figure 2 we show the results of our parametric study at Pr = 1. We plot surface temperature T(x,1), velocity u(x,1), and the surface deflection h(x) corresponding to five different values of Re (or Ma). For Re less than about 1000, it is seen from Figure 2a that the surface temperature gradient at the hot corner $T_x(-1/2,1)$ is greater than the conduction value of -1, i.e a decreased surface vorticity at the hot corner. At these relatively low values of Re, Figure 2b indicates that the surface velocity increases monotonically from zero and drops back smoothly to zero at the cold corner. The associated surface deflection plot in Figure 2c shows that there are two peaks in h(x) which decrease

in magnitude and move towards the corners with increasing Re. With Re (or Ma) increasing above 1000 however, $T_x(-1/2,1)$ is less than -1 and decreasing, u(x,1) exhibits two peaks and h(x) showing a more or less flat depression on an increasing length of the free surface near the hot (left) boundary. It is also observed that the surface elevation near the cold corner is increasing with Re. From these features it may be concluded that a boundary layer regime is reached for Re (or Ma) greater than about 1000.

The streamlines, vorticity and temperature fields corresponding to Re = Ma = 10^4 are shown in Figure 3. From this Figure it may be concluded that the limiting flow field at large values of Re (or Ma) will consist of an irrotational, isothermal core with boundary layers forming on the four boundaries. The corner eddies predicted by Moffatt (1964) are present in Figure 3a, while the vorticity is discontinuous near the corners in accord with equation (3.2). The sharpest gradients occur near the cold corner as evident in Figure 3c.

Of interest is the total heat transport, or the Nusselt number, defined by

$$Nu_{\pm} = {}_0\int^1 -T_x(\pm 1/2,y)\, dy \quad , \tag{4.2}$$

As noted above, $Nu_+ = Nu_-$ to within 1%. In Figure 4 we show the variation of T_x along the hot and cold walls from which it follows that while all of the hot boundary participates in the heat transfer process, only a "small" cold corner region contributes to most of the transfer. This picture will be validated in section 5.

The vigor of the convective motion is indicated by the magnitudes of the heat transfer, flow circulation (ψ_{max}) and maximum vorticity (ω_{max}). Figure 5 is a logarithmic plot of the variation of $Nu = (Nu_- + Nu_+)/2$, $-\omega_{max}$ and $-\psi_{max}$ with Re, where $\omega_{max} = T_x(1/2,1)$ for all the cases with Pr = 1 that we computed. From Figure 5 it may be concluded that

$$-\omega_{max} \sim O(Re^{2/3}) \quad , \tag{4.3}$$

$$Nu \sim O(Re^{1/3}) \quad , \tag{4.4}$$

$$-\psi_{max} \sim O(Re^{-1/3}) \quad , \tag{4.5}$$

as $Re \rightarrow \infty$. We show in Section five how these asymptotic relations are in agreement with a possible consistent boundary layer structure for this flow.

5. Structure of boundary layers; Pr = 1

Below we develop a self-consistent picture of the boundary layer structure which exists asymptotically as Re $\to \infty$. We show that, beginning with the key assumption that surface vorticity becomes independent of Re as Re $\to \infty$, all of the available numerical evidence is in agreement with the inferred scalings. The first region of interest is the boundary layer near the free surface.

Free surface layer

Here $x \sim O(1)$. The assumption $\omega \sim O(1)$, which follows from the boundary condition (2.9a) and Figure 2c, together with the required balance of diffusion and convection lead to the free surface transformation:

$$x = \bar{x} \quad ; \quad y = 1 - Re^{-1/3}\bar{y} \quad , \qquad (5.1a,b)$$

$$u = Re^{-1/3}\bar{u}(\bar{x},\bar{y}) \; ; \; v = Re^{-2/3}\bar{v}(\bar{x},\bar{y}) \; ; \; \psi = Re^{-2/3}\bar{\psi}(\bar{x},\bar{y}) \; , \qquad (5.1c,d,e)$$

$$p = Re^{1/3}\bar{p}(\bar{x},\bar{y}) \quad , \qquad (5.1f)$$

$$T = \bar{T}(\bar{x},\bar{y}) \quad . \qquad (5.1g)$$

Equation (5.1c) implies a surface velocity decreasing with Re in qualitative agreement with Figure 2b. The boundary layer equations, to leading order become

$$\bar{u}_{\bar{x}} + \bar{v}_{\bar{y}} = 0 \qquad (5.2a)$$

$$\bar{u}\bar{u}_{\bar{x}} - \bar{v}\bar{u}_{\bar{y}} = -\bar{p}_{\bar{x}} + \bar{u}_{\bar{y}\bar{y}} \quad , \qquad (5.2b)$$

$$0 = p_y \quad , \qquad (5.2c)$$

$$\bar{u}\bar{T}_{\bar{x}} - \bar{v}\bar{T}_{\bar{y}} = Pr^{-1}\bar{T}_{\bar{y}\bar{y}} \quad . \qquad (5.2d)$$

These are the usual boundary layer equations. The known boundary conditions are

$$\bar{y} = 0 \; : \; \bar{v} = \bar{T}_{\bar{y}} = 0 \; ; \; -\bar{u}_{\bar{y}} = \bar{T}_{\bar{x}} \quad . \qquad (5.3a,b,c)$$

Matching conditions for $\bar{y} \to \infty$ with a core solution and initial conditions for $\bar{x} \to -1/2$ must be provided.

Core region

Formally, the limiting equations in the core are

$$(\underline{V}.\nabla)\omega = 0 \quad , \tag{5.4a}$$

$$(\underline{V}.\nabla)T = 0 \quad . \tag{5.4b}$$

Thus , in principle, ω and T are constants along streamlines. Figures 2b and 2c indicate that the limiting core flow is isothermal (at some T_c) and irrotational. The pressure field is then found from the Bernoulli equation

$$p + Re\ V^2/2 = \text{constant} \quad . \tag{5.5}$$

Matching with the free surface layer indicates that

$$p \sim O(Re^{1/3}) \quad ; \quad V \sim O(Re^{-1/3}) \quad , \tag{5.6a,b}$$

so that the core streamfunction

$$\psi \sim O(Re^{-1/3}) \quad . \tag{5.7}$$

This is consistent with equation (4.6) and Figure 4.

Cold corner region

This stagnation point flow region is where most of the heat transfer on the cold boundary occurs (Figures 2a, 3c, 4b) and where the largest vorticity is generated. The horizontal free surface flow turns in this region as u(x,1) drops sharply to zero (Figure 2b). The y extent and the amount of flow in this region are determined by those in the free surface region. In addition, the required convection-diffusion balance leads to the cold corner scalings

$$y = 1 - Re^{-1/3}\ \tilde{y} \quad ; \quad x = 1/2 - Re^{-2/3}\ \tilde{x} \quad , \tag{5.8a,b}$$

$$u = Re^{-1/3}\ \tilde{u}(\tilde{x},\tilde{y}) \quad ; \quad v = \tilde{v}(\tilde{x},\tilde{y}) \quad ; \quad \psi = Re^{-2/3}\ \tilde{\psi}(\tilde{x},\tilde{y}) \tag{5.8c,d,e}$$

$$\omega = Re^{2/3}\ \tilde{\omega}(\tilde{x},\tilde{y}) \quad , \tag{5.8f}$$

$$p = Re^{1/3}\ \tilde{p}(\tilde{x},\tilde{y}) \quad , \tag{5.8g}$$

$$T = \tilde{T}(\tilde{x},\tilde{y}) \quad . \tag{5.8h}$$

The leading order equations, boundary and matching conditions become

$$\tilde{u}_{\tilde{x}} + \tilde{v}_{\tilde{y}} = 0 \qquad (5.9a)$$

$$-\tilde{u}\tilde{u}_{\tilde{x}} + \tilde{v}\tilde{u}_{\tilde{y}} = \tilde{p}_{\tilde{x}} + \tilde{u}_{\tilde{x}\tilde{x}} \ , \qquad (5.9b)$$

$$-\tilde{u}\tilde{v}_{\tilde{x}} - \tilde{v}\tilde{v}_{\tilde{y}} = \tilde{v}_{\tilde{x}\tilde{x}} \ , \qquad (5.9c)$$

$$-\tilde{u}\tilde{T}_{\tilde{x}} - \tilde{v}\tilde{T}_{\tilde{y}} = Pr^{-1}\tilde{T}_{\tilde{x}\tilde{x}} \ , \qquad (5.9d)$$

$$\tilde{x} = 0 : \ \tilde{u} = \tilde{v} = 0 \ ; \ \tilde{T} = -1/2 \ , \qquad (5.9e,f,g)$$

$$\tilde{x} \to \infty : \ \tilde{v} \to 0 \ , \ \tilde{u}(\tilde{x}\to\infty,\tilde{y}) \sim \tilde{u}(\tilde{x}\to 1/2,\tilde{y}) \ . \qquad (5.9h,i)$$

These quantities can not satisfy the initial conditions on $\tilde{y} = 0$ since $\tilde{u}_{\tilde{y}} \sim O(1)$ while $\tilde{T}_{\tilde{x}} \sim O(Re^{2/3})$. Thus, there will be a corner subregion where

$$1/2 - x \sim O(Re^{-2/3}) \ , \qquad (5.10a)$$

$$1 - y \sim O(Re^{-1}) \ , \qquad (5.10b)$$

$$\psi \sim O(Re^{-4/3}) \ , \qquad (5.10c)$$

$$T \sim O(1) \ , \qquad (5.10d)$$

It should be noted that (5.10c) is a consequence of higher order free surface layer, while (5.10b) is necessary to satisfy the vorticity balance on the free surface.

Equations (5.8) is in complete agreement with Figures 3b, 4, indicating that most of the heat transfer on the cold wall is within the corner region. In addition, it follows from equation (4.3) that

$$Nu = {}_0\int^1 -T_x(1/2,y)\, dy \ ,$$
$$\sim Re^{1/3} \, {}_0\int^{\infty} \tilde{T}_{\tilde{x}}(0,\tilde{y})\, d\tilde{y} \ , \qquad (5.11)$$

which, again, is in agreement with Figure 5.

The existence of these regions with various asymptotic scales (see equations 5.1, 5.8 and 5.10), is very demanding on the computational mesh. This is particularly so at extreme values of Pr.

Figure 6 gives a sketch of the important boundary layer regions, and the important scalings therein. The boundary layer equations are difficult to solve, however, because of the difficulty in conveniently representing solutions to equations (5.4) in the core. Thus we expect that the boundary layer problem may be as difficult to solve as the original equations.

6. Numerical results; Pr ≠ 1

Equations (2.2) and (4.1) show that convection of vorticity is stronger (weaker) than convection of energy according to Pr<1 (Pr>1). The influence of Pr on the motion is ascertained from a sequence of computations with Pr = 0.05, 0.1, 1, 10 and 50. The largest value of Re or Ma attainable with reasonable accuracy was 50,000.

Figures 7a,b are plots of the surface temperature corresponding to Pr = 0.1 and 50 at various values of Re. It is seen that, with increasing Re, the surface vorticity at the hot corner first decreases, and then begins to increase monotonically with further increase in Re. This is similar to the case Pr = 1 in Figure 2a. The surface velocity corresponding to the parameter values of Figures 7a,b are shown in Figures 8a,b. It is observed that a two-peak structure is eventually approached at sufficiently large Re (or Ma). It is important to note; Figure 8b, that at appropriately low values of Re (depending on Pr) that for Pr > 1 the motion is faster near the hot corner than almost every where on the free surface except in the readily developed thermal (and vorticity layer at the cold corner). The opposite is true for Pr < 1 and low Re; Figure 8a, where convection is expected to dominate near the cold corner.

The influence of Pr on the pattern of circulation is evident from Figures 9a,b where show the streamlines of the thermocapillary motion corresponding to Pr, Re and Ma values of 0.05; 1000; 50 and 50; 200; 10,000. At sufficiently low Re it is seen that the point where $-\psi_{max}$ occurs is close to the cold corner when Pr < 1, while for Pr > 1 this point occurs near the hot corner. Thus, again, it is concluded that convective effects are more important at the hot (cold) corner according to Pr > 1 (< 1) at appropriate low values of Re. With increasing Re, however, the pattern of motion is similar to that for Pr = 1 in Figure 3a. This behavior with Pr was also found by Fu & Ostrach (1983) in their axisymmetric half-zone model.

Plots of $-\psi_{max}$, Nu and $-\omega_{max}$ versus Re, similar to those in Figures 5a,b,c for Pr = 1, show that the asymptotic estimates given in equations (4.4), (4.5) and (4.6) are applicable with Pr = 1. This is also indicative that the character of the motion becomes independent of Pr at sufficiently large Re.

The most remarkable influence of Pr on thermocapillary convection is found on the shape of the free surface. Figures 10a,b show h(x) for the parameter values of Figures 7a,b and 8a,b. It is seen that for Pr > 1, the region of strong motion near the hot corner is accompanied by sufficient low pressure that the largest depression exceeds the largest elevation. At Pr < 1 however, there is a build up of pressure sufficient to produce a secondary elevation near the hot corner.

It is of interest to note that, for all the cases considered, |h(x)| is small, (Figures 2c, 10), indicating that the range of capillary numbers for which the surface deflection is accurately given by perturbation in Ca may be rather large.

7. Concluding remarks

We have presented the results of a reasonably complete study of thermocapillary convection in a square cavity. Our accurate computational procedure allows us to consider situations with large Re and Ma, and thus observe the formation of boundary layers, in particular at the cold stagnation point region. This boundary layer structure is shown to be consistent with an asymptotic theory valid as $Re \rightarrow \infty$.

We encountered no difficulty in computing two-dimensional steady states by time-like iterations. It is also felt, from numerical experiments, that such steady motions continue to exist at yet higher values of Re and Ma. Since, from previous experimental work and from the analysis of Smith & Davis (1983a), it is expected that oscillatory motions will prevail at some "supercritical" Re and Ma, it is conjectured that such an unsteady motion is three-dimensional. It seems that there is no convenient method to study the instability of the solutions we computed on the finite difference grid to three-dimensional disturbances. Thus, further progress in the study of this phenomena must be both three-dimensional and time dependent.

Acknowledgment

We wish to acknowledge the partial support of NASA through contract NAS8-33881. E. M. was partially supported through a DAAD scholarship for one year study at Stanford. We are also grateful to the Center for Large Scale Scientific Computation, funded by the Office of Naval Research Contract N00014-82-K-0335 for the use of their computer facilities.

Table I
Influence of finite-difference grid on the solution

Pr	Re	M x N*	Nu_-	Nu_+	$-\psi_{max} \times 10^2$	$-\omega_{max}$
0.05	5×10^4	62 x 54	2.120	2.131	0.174	14.37
		70 x 60	2.161	2.151	0.180	14.44
0.1	5×10^4	62 x 54	2.937	2.957	0.168	29.04
		70 x 60	2.980	2.981	0.175	28.95
1	5×10^3	65 x 65	3.459	3.448	0.370	28.72
		80 x 80	3.454	3.447	0.373	31.20
		62 x 54	3.420	3.412	0.366	38.37
50	5×10^2	62 x 54	4.895	4.898	0.155	139.4
		70 x 60	4.894	4.896	0.155	139.7

* M and N are the number of grid points in the x and y directions respectively. The 65 x 65 and 80 x 80 grids are uniform while the 62 x 54 and the 70 x 60 grids are graded.

REFERENCES

1. Fu, B. & Ostrach, S. 1982 FTAS/TR-82-169, Case Western Reserve University.

2. Gottlieb, D & Orszag, S. Numerical Analysis of Spectral Methods: Theory and Applications Soc. Ind. App. Math., Philadelphia, 1977.

3. Kamotani, Y., Ostrach, S. & Vargas, M. 1984 J. Crystal Growth. 66, 83.

4. Moffatt, H. K. 1964 J. Fluid Mech. 18, 1.

5. Ostrach, S. 1982 Ann. Rev. Fluid Mech. 14, 313.

6. Patankar, S. V. 1981 Numer. Heat Transfer 4, 409.

7. Peisser, F., Schwabe, D. & Scharmann, A. J. 1983 Fluid Mech. 126, 545.

8. Schwabe, D. 1981 Physiochem. Hydrodyn. 2, 263.

9. Sen, A. K. & Davis, S. H. 1982 J. Fluid Mech. 121, 163.

10. Smith, M. K. & Davis, S. H. 1983a J. Fluid Mech. 132, 119.

11. Smith, M. K. & Davis, S. H. 1983b J. Fluid Mech. 132, 145.

12. Strani, M., Piva, R. & Graziani, G. 1983 J. Fluid Mech. 130 347.

Figure captions

- Figure 1. Thermocapillary flow at Pr = 1 and Re = 1000. a) Streamlines at equal increments of circulation. The motion is clockwise with $-\psi_{max}$ = 0.0048. b) Isotherms at equal increments. c) Iso-vorticity contours. ω = -1.0 and -11.79 at the top hot (left) and cold (right) corners, respectively. The largest positive ω is 7.3.

- Figure 2. a) Surface temperature corresponding to Pr = 1 and Re = 100, 500, 1,000, 5,000 and 10,000. b) Associated surface velocity, and c) surface deflection.

- Figure 3. Same as Figure 1 but with Re = 10,000. Here $-\psi_{max}$ = 0.003; ω = -2.4 and -60.2 at the top hot and cold corners, respectively; and the largest value of ω is 10.5.

- Figure 4. Variation with y of T_x on the a) hot boundary, and b) cold boundary at Pr = 1 and Re = 1,000, 5,000 and 10,000.

- Figure 5. Variation with log Re of log $(-\psi_{max})$, log $(-\omega_{max})$ and log Nu. Also shown are straight lines with slopes -1/3, 2/3 and 1/3.

- Figure 6. Sketch of the important surface layer regions. The following are the scalings in regions I, II, III and the core.

	u	v	ψ	ω	T_x
I:	$Re^{-1/3}$	$Re^{-2/3}$	$Re^{-2/3}$	1	1
II:	$Re^{-1/3}$	1	$Re^{-2/3}$	$Re^{2/3}$	$Re^{2/3}$
III:	$Re^{-1/3}$	$Re^{-2/3}$	$Re^{-4/3}$	$Re^{2/3}$	$Re^{2/3}$
core:	$Re^{-1/3}$	$Re^{-1/3}$	$Re^{-1/3}$	1	1

- Figure 7. Surface temperature T(x,1) at a) Pr = 0.1 and Re = 10^3, 10^4, 2 x 10^4 and 5 x 10^4. b) Pr = 50 and Re = 20, 100, 200 and 500.

- Figures 8a,b. Associated surface velocity u(x,1) at the parameter values of Figures 7a,b, respectively.

- Figure 9. Streamlines corresponding to a) Pr = 0.05 and Re = 1000; $-\psi_{max}$ = 0.0088, and b) Pr = 50 and Re = 200; $-\psi_{max}$ = 0.0019.

- Figure 10a,b. Surface deflection at the parameter values of Figures 7a,b, respectively.

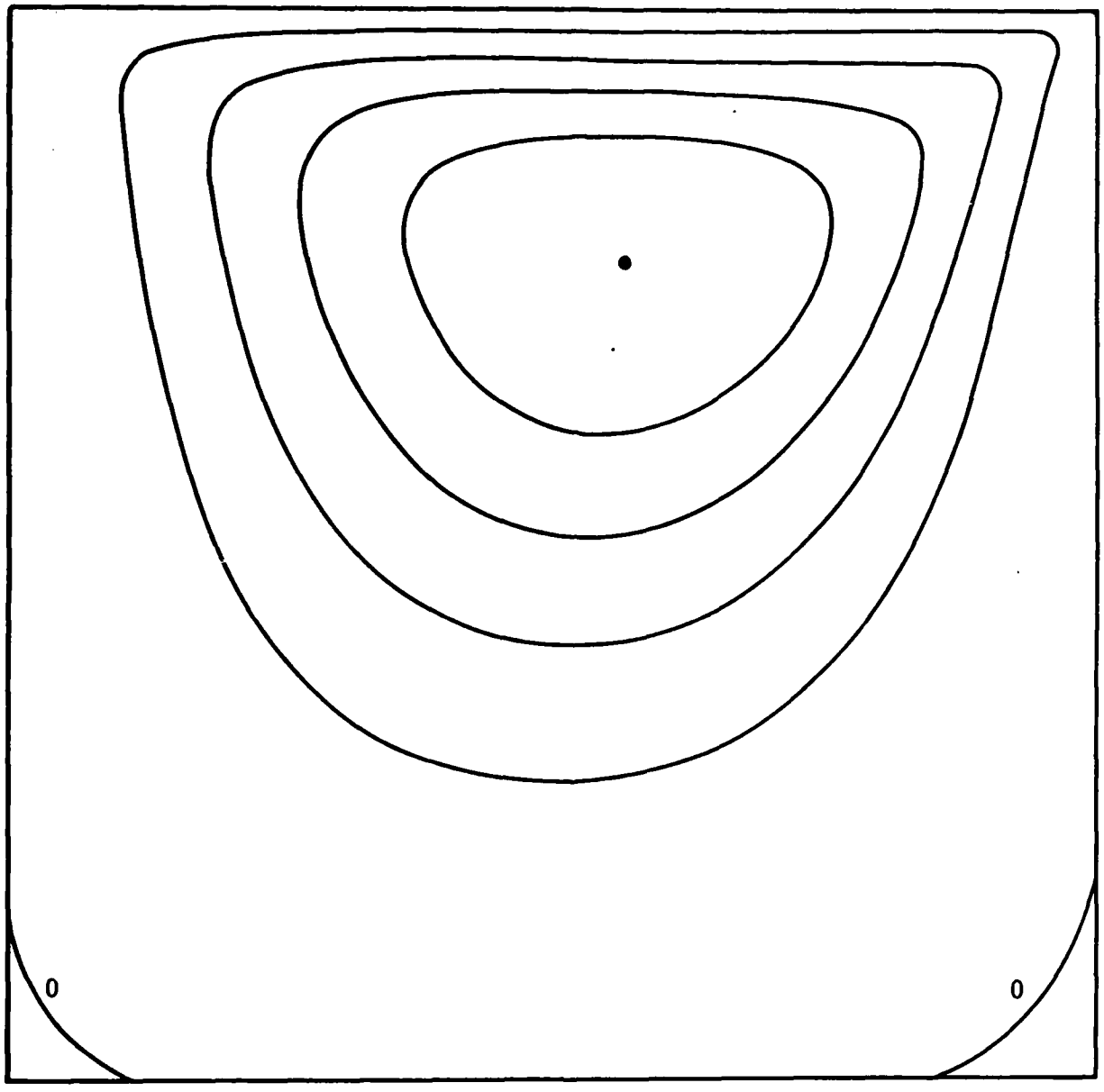

Figure 1a

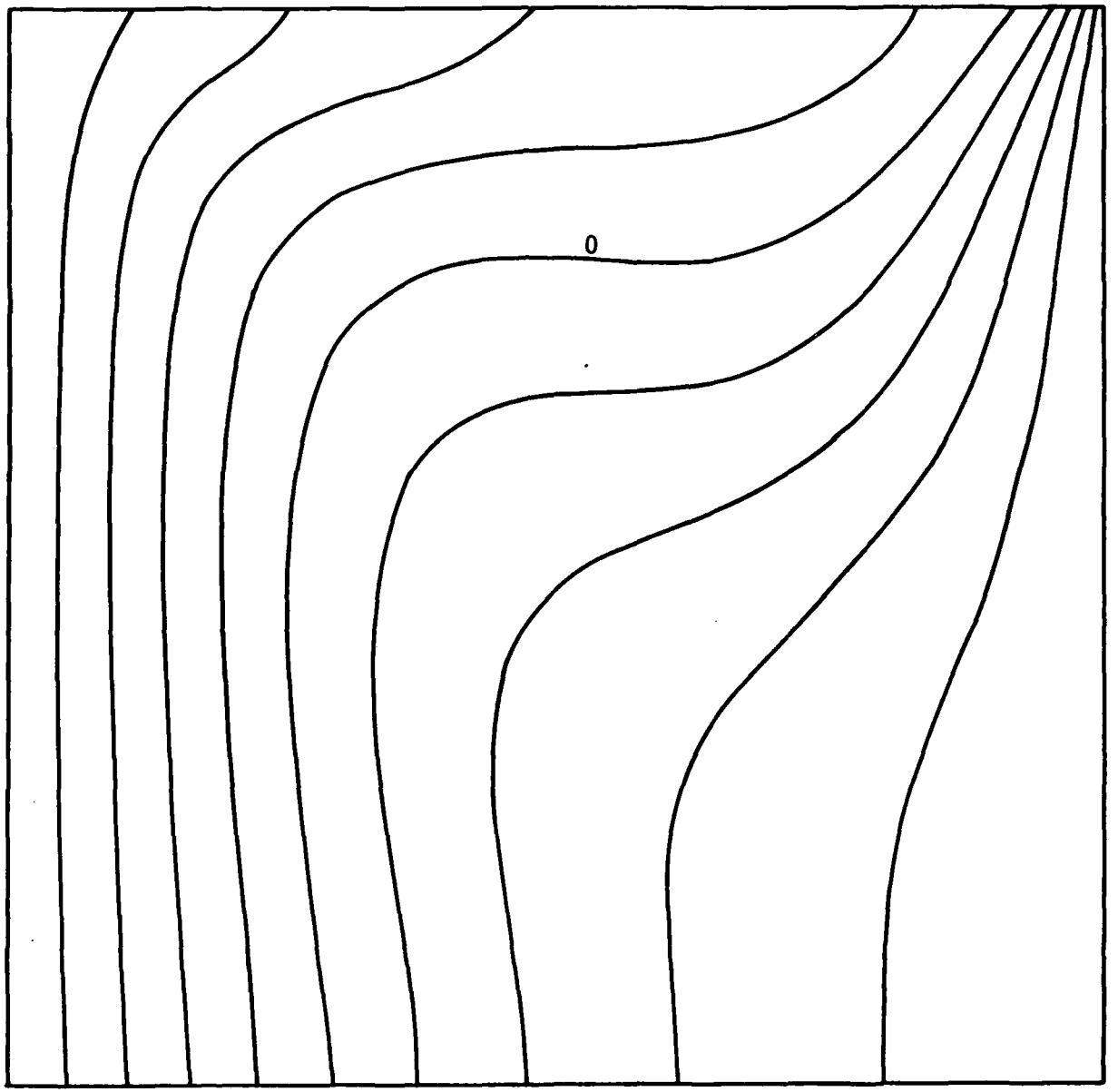

Figure 1b

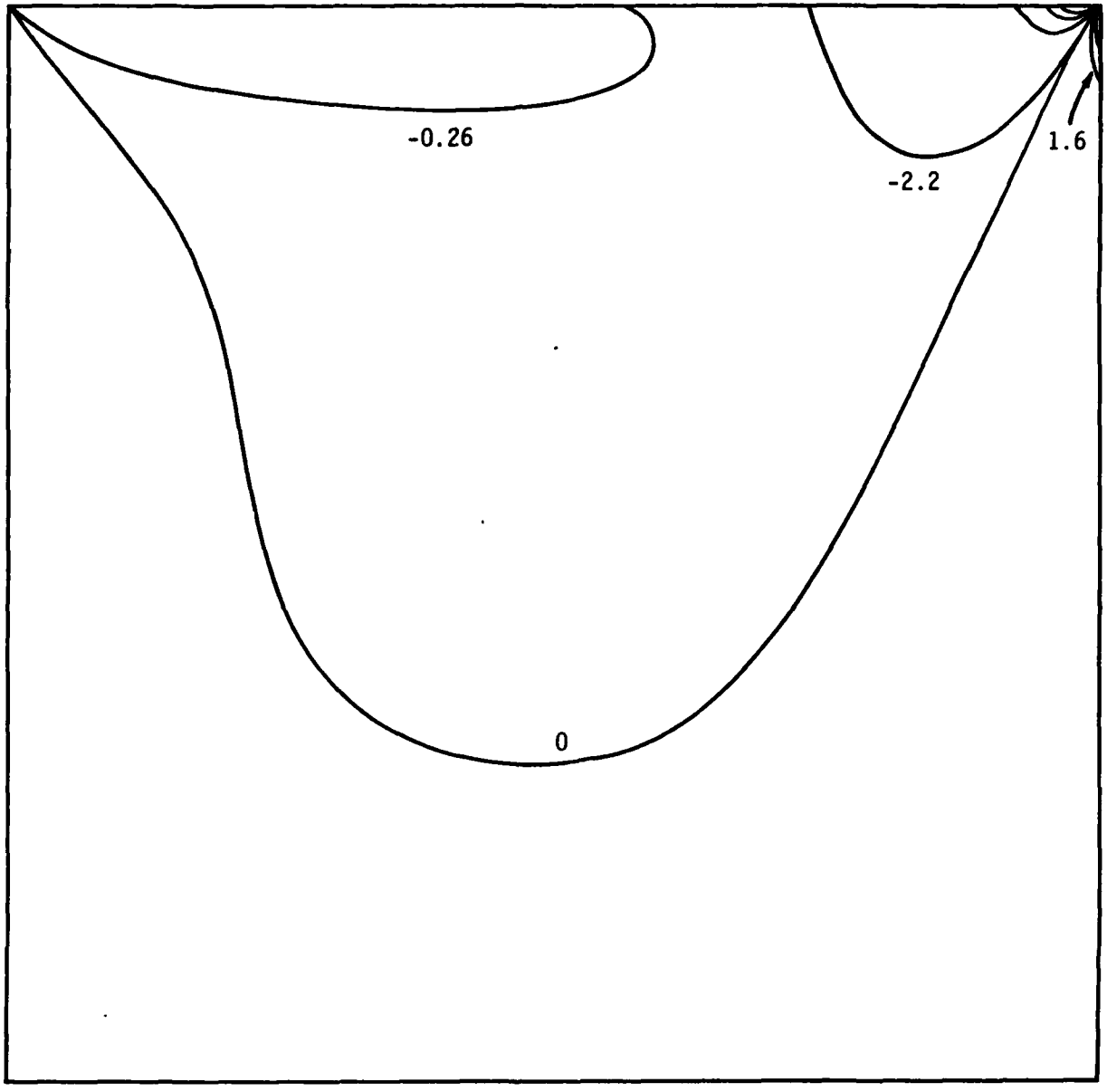

Figure 1c

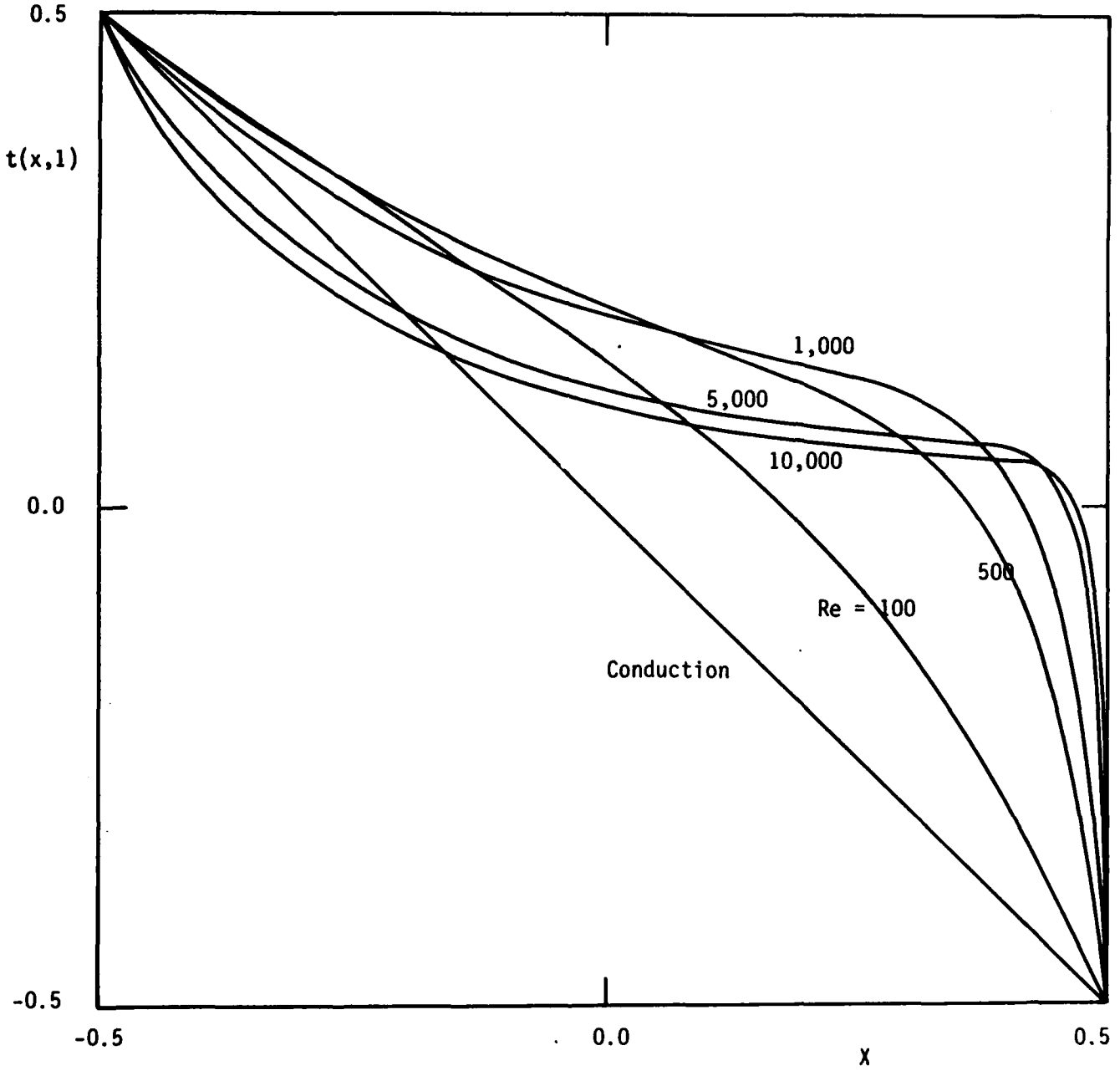

Figure 2a

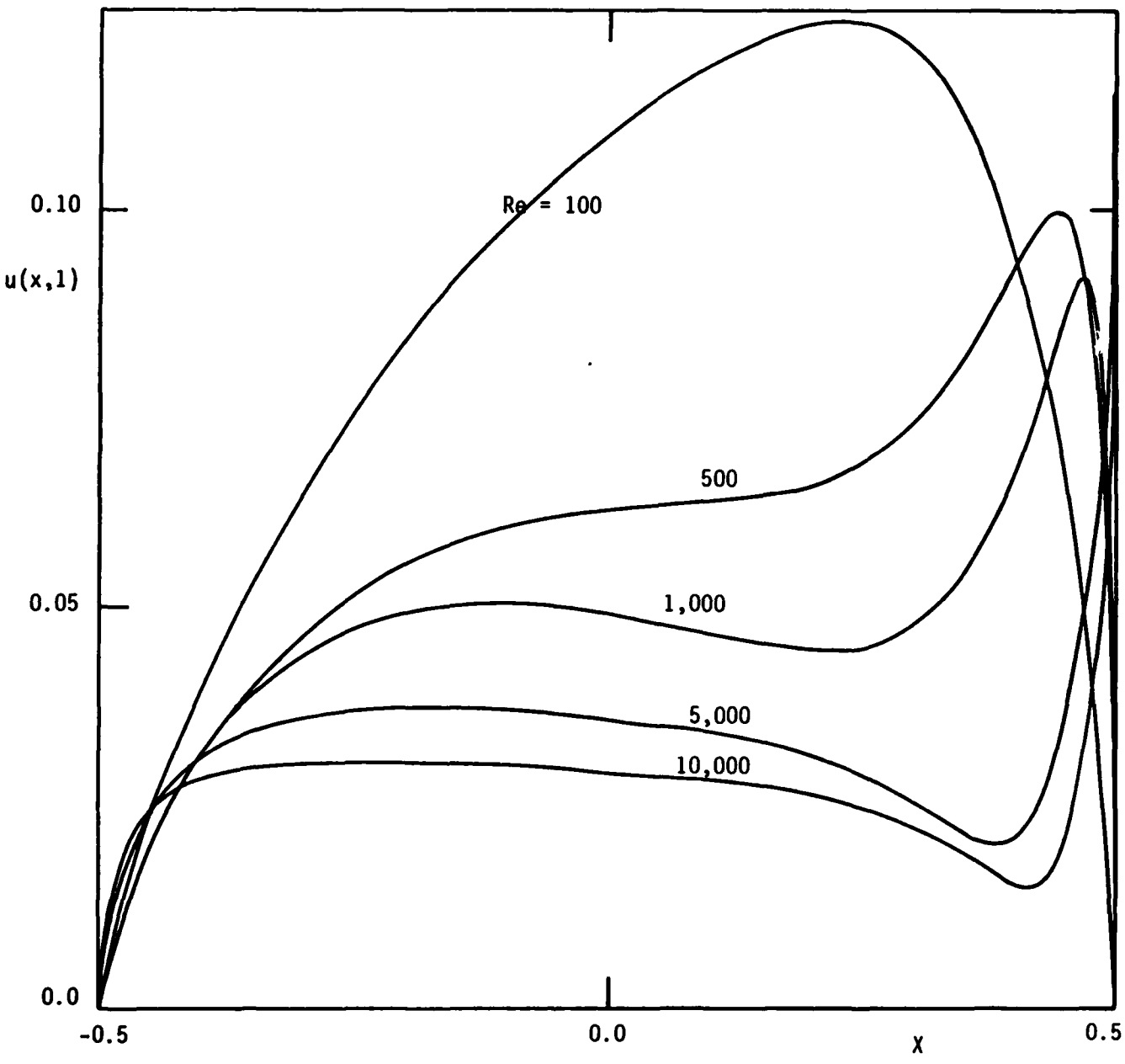

Figure 2b

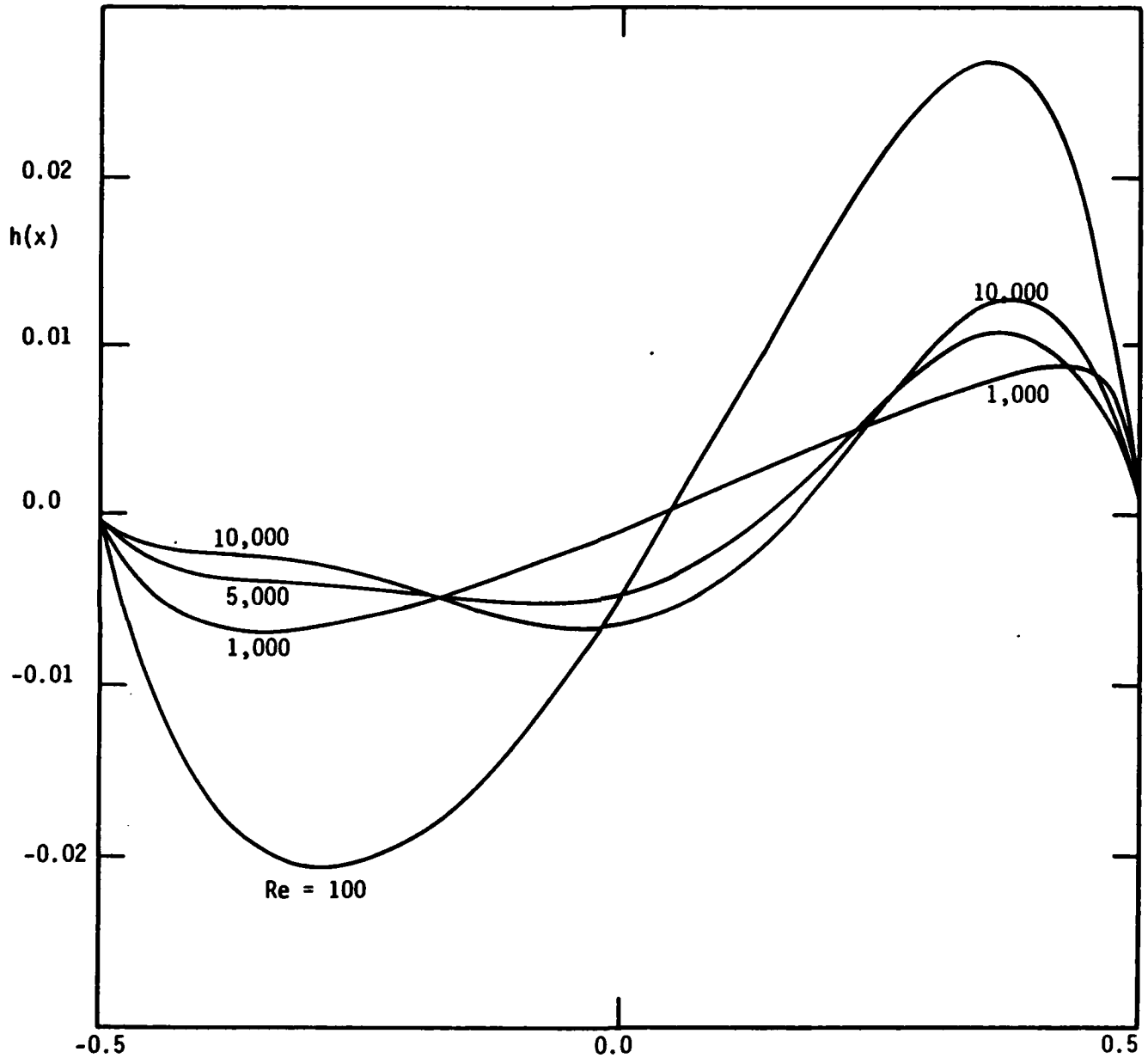

Figure 2c

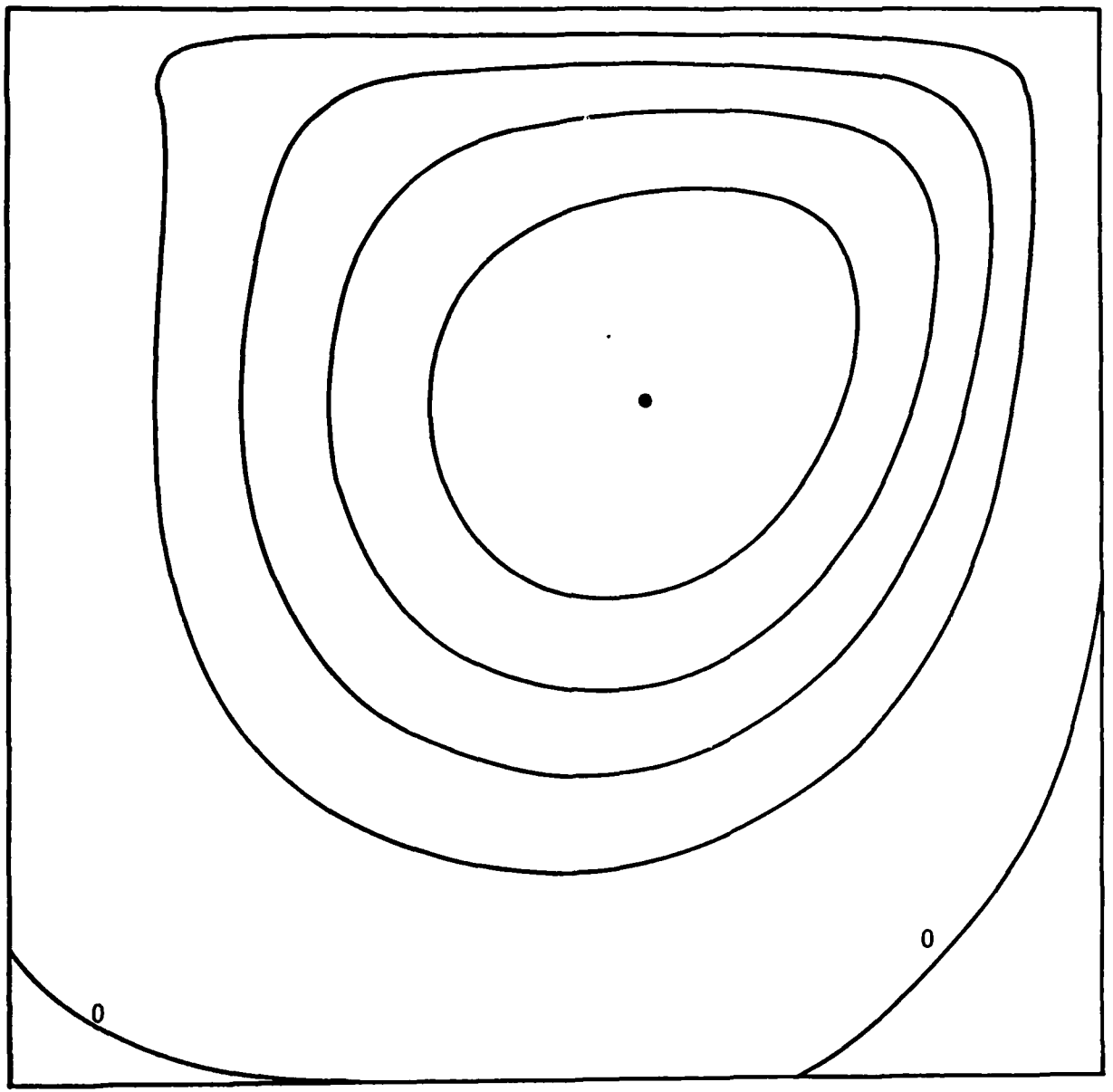

Figure 3a

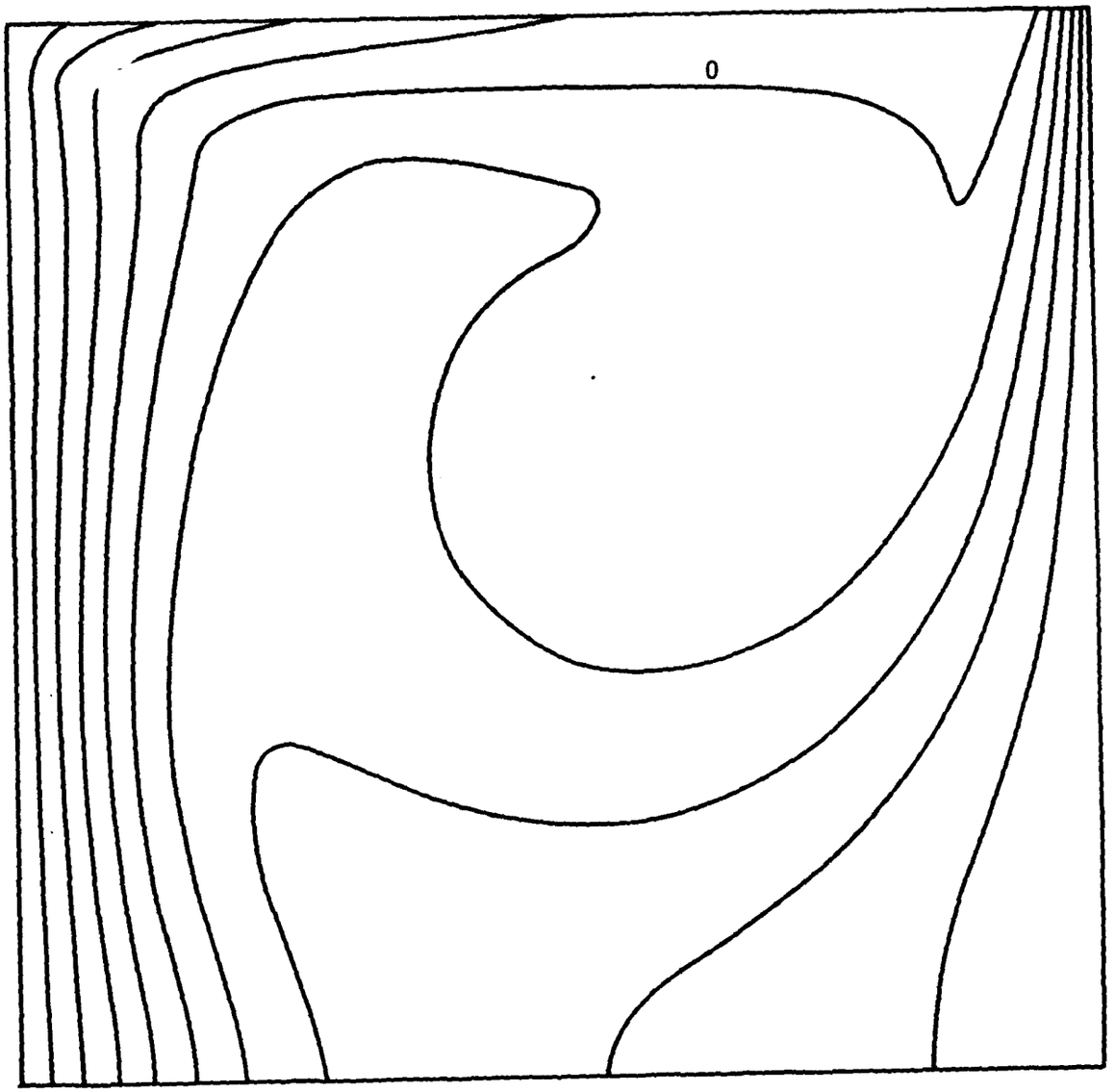

Figure 3b

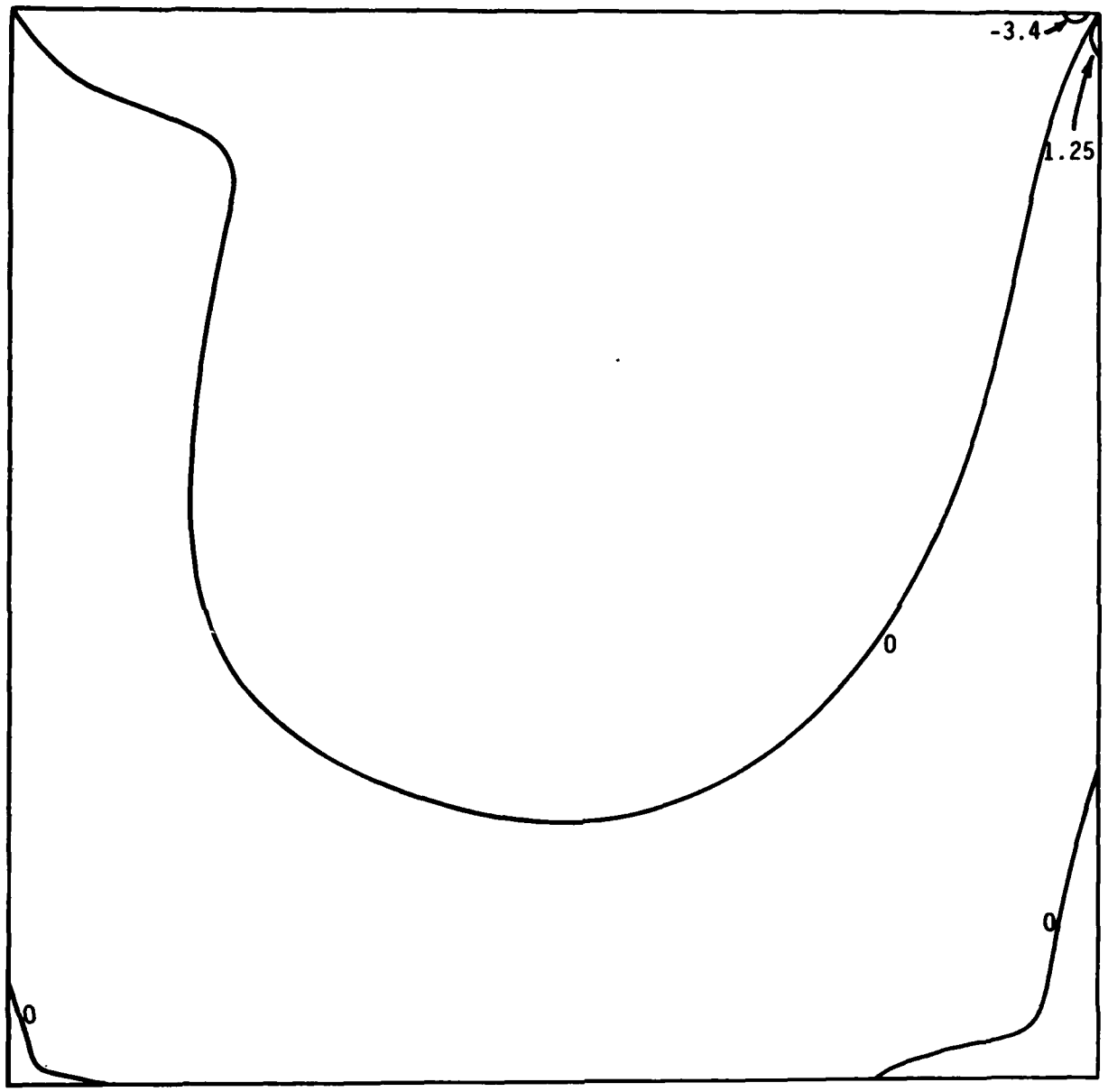

Figure 3c

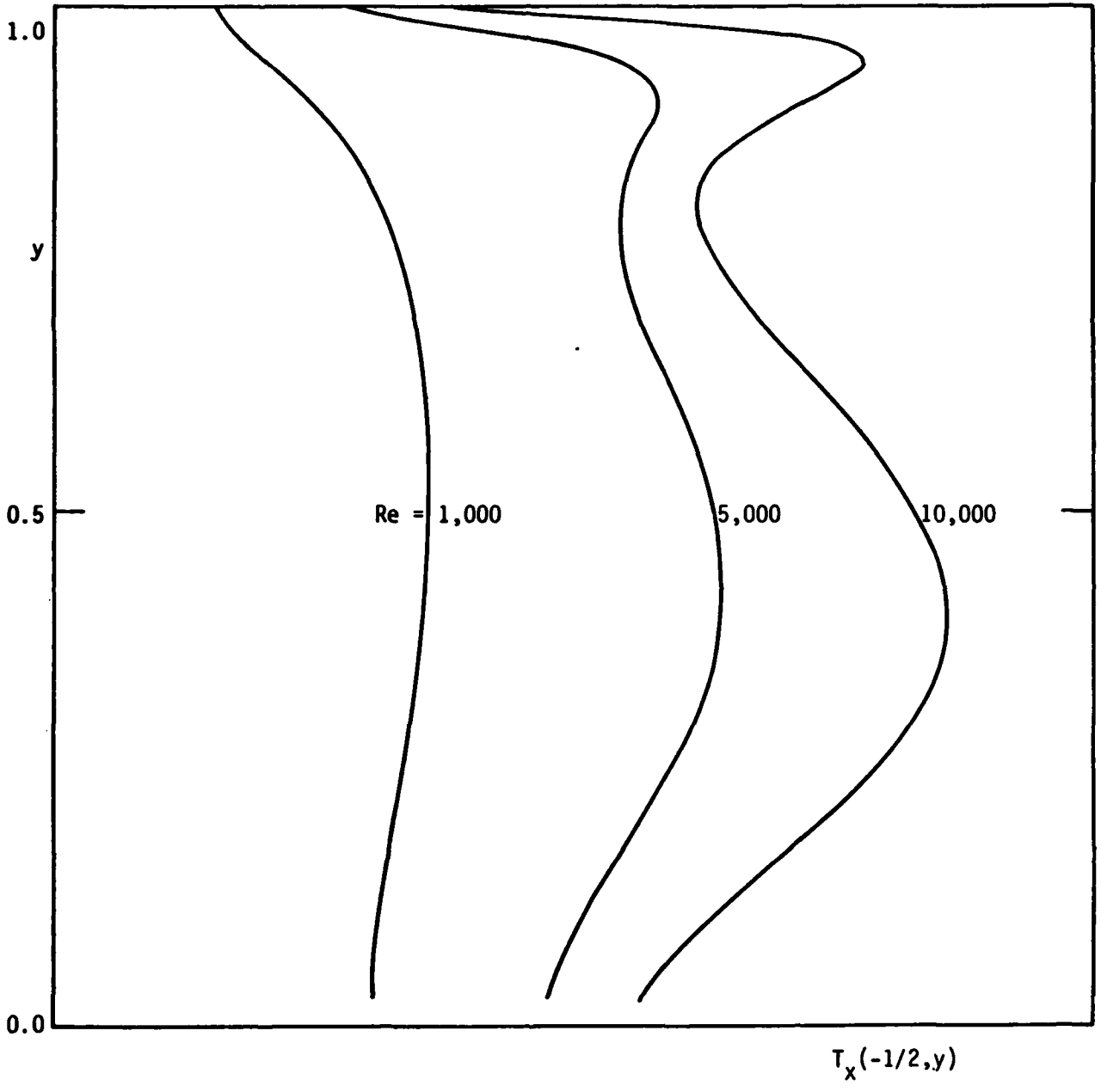

Figure 4a

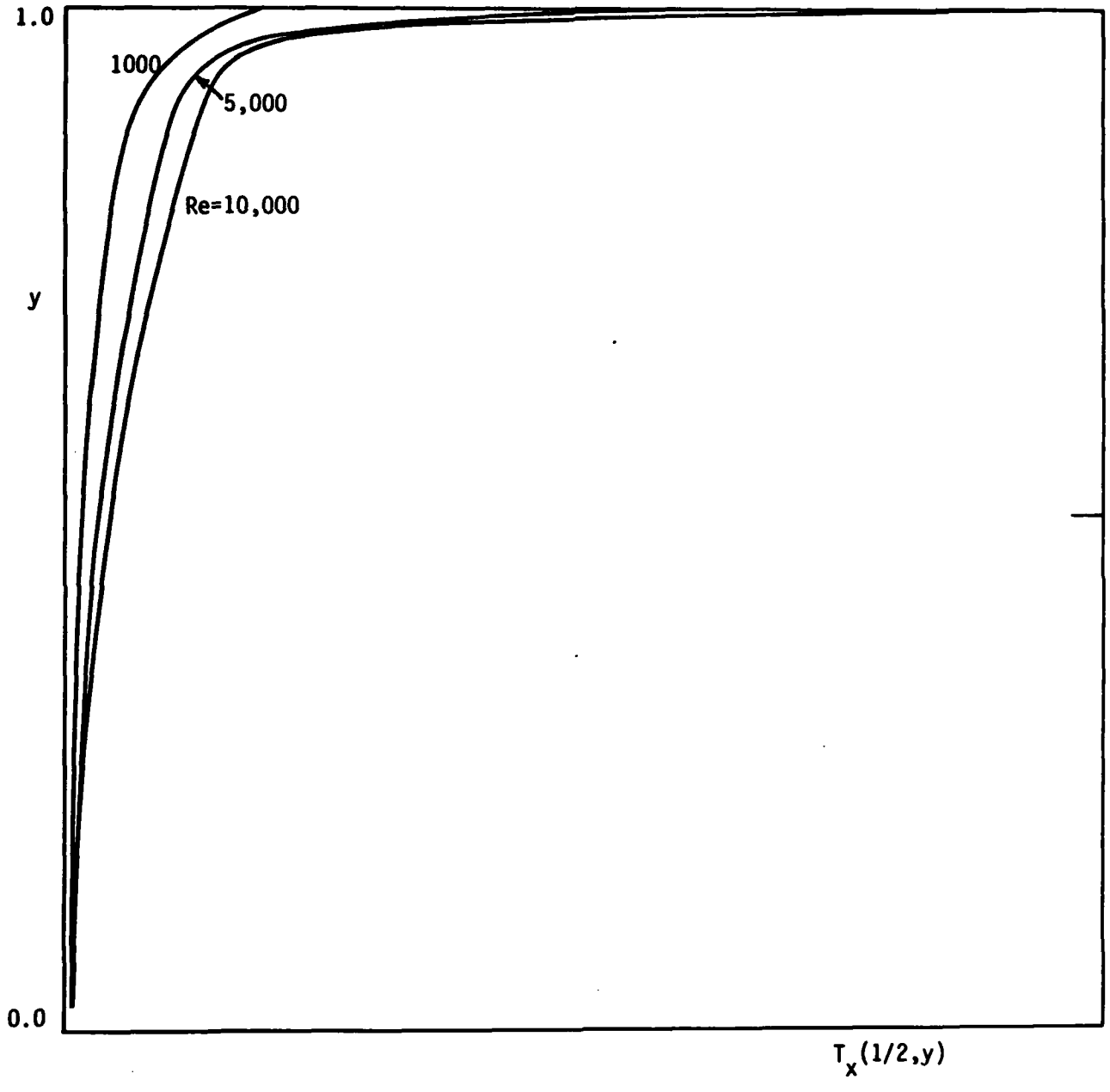

Fibure 4b

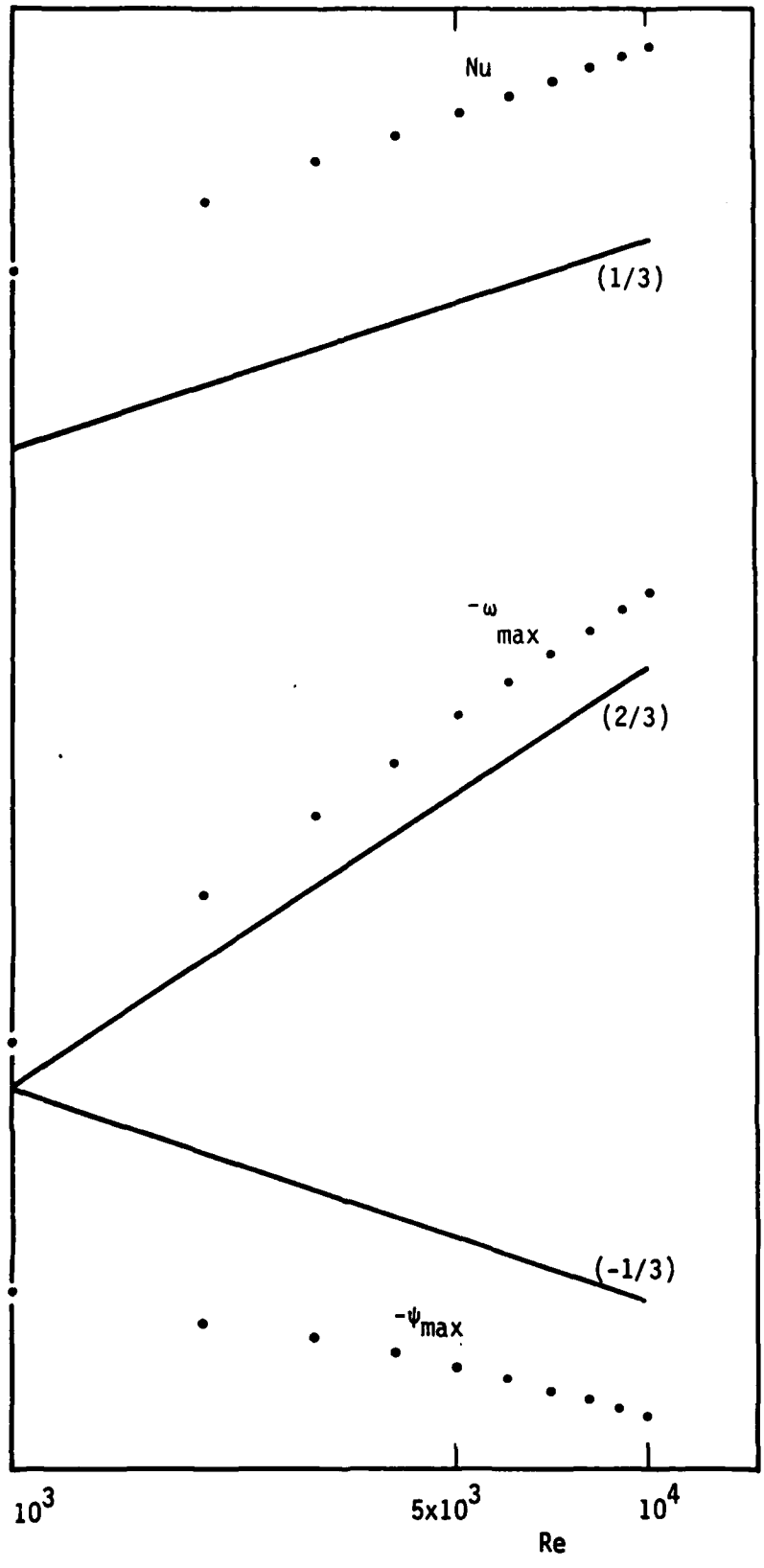

Figure 5

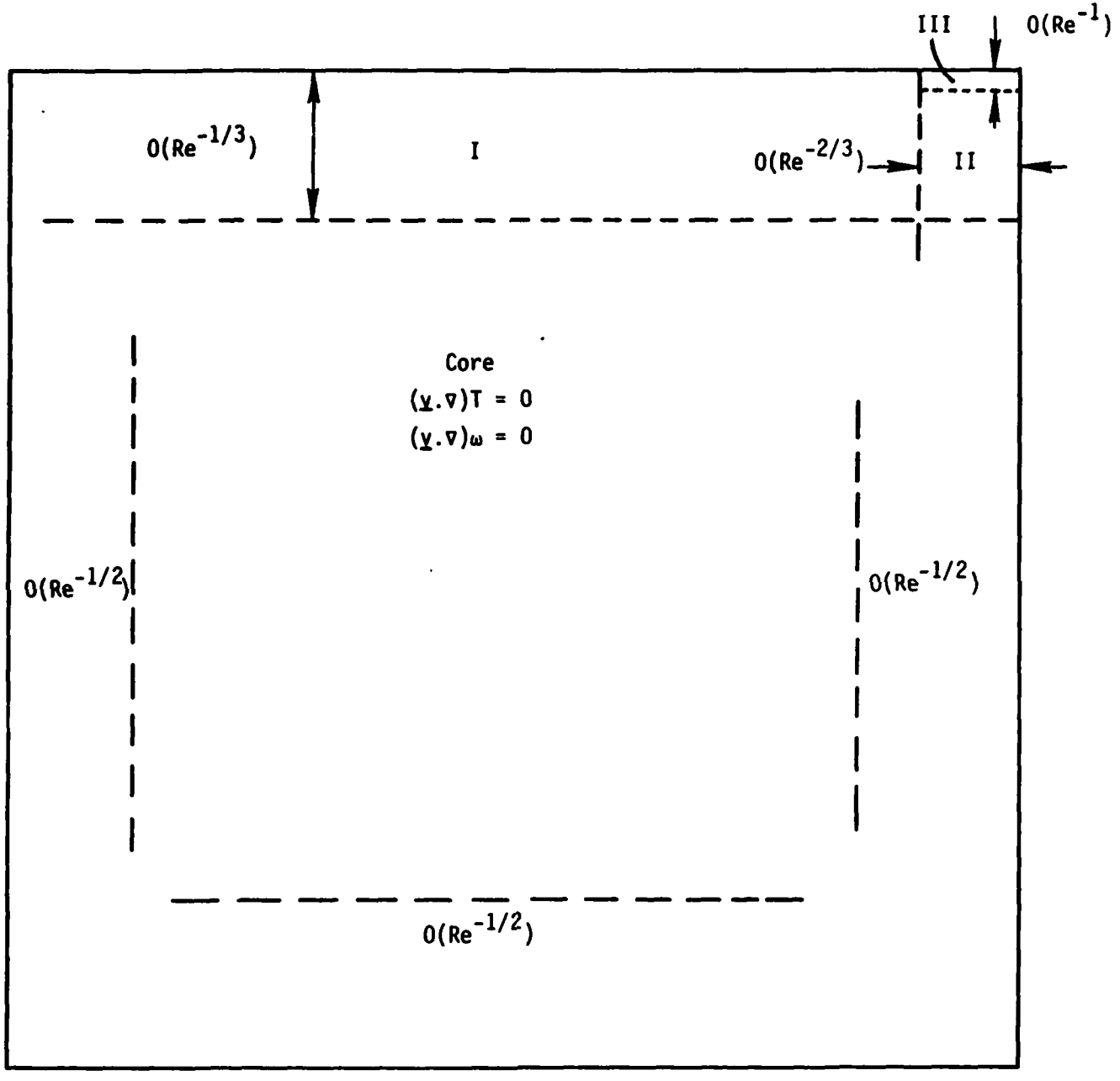
III
$O(Re^{-1})$
$O(Re^{-1/3})$
I
$O(Re^{-2/3})$
II
Core
$(\underline{v}.\nabla)T = 0$
$(\underline{v}.\nabla)\omega = 0$
$O(Re^{-1/2})$
$O(Re^{-1/2})$
$O(Re^{-1/2})$

Figure 6

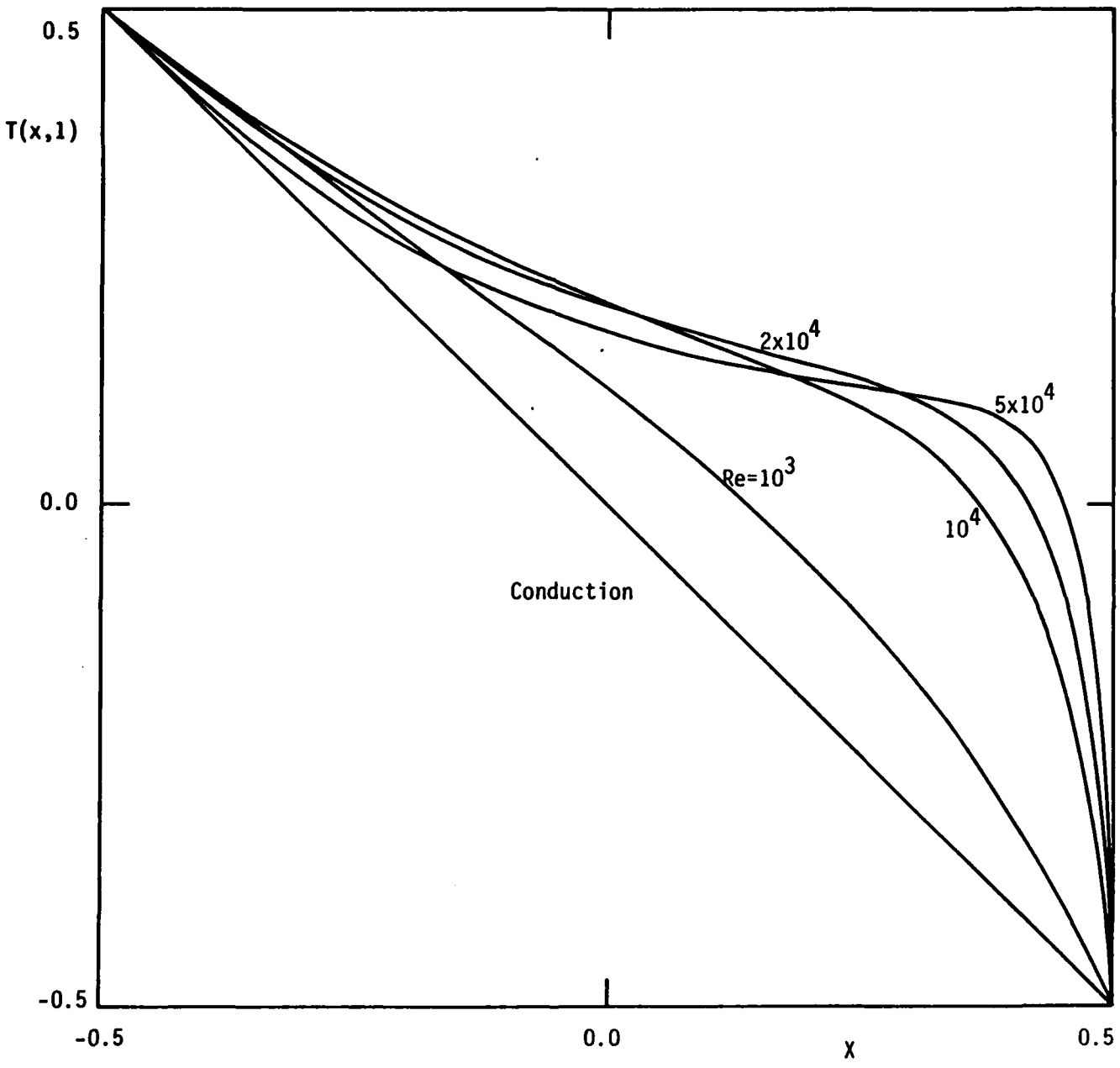

Figure 7a

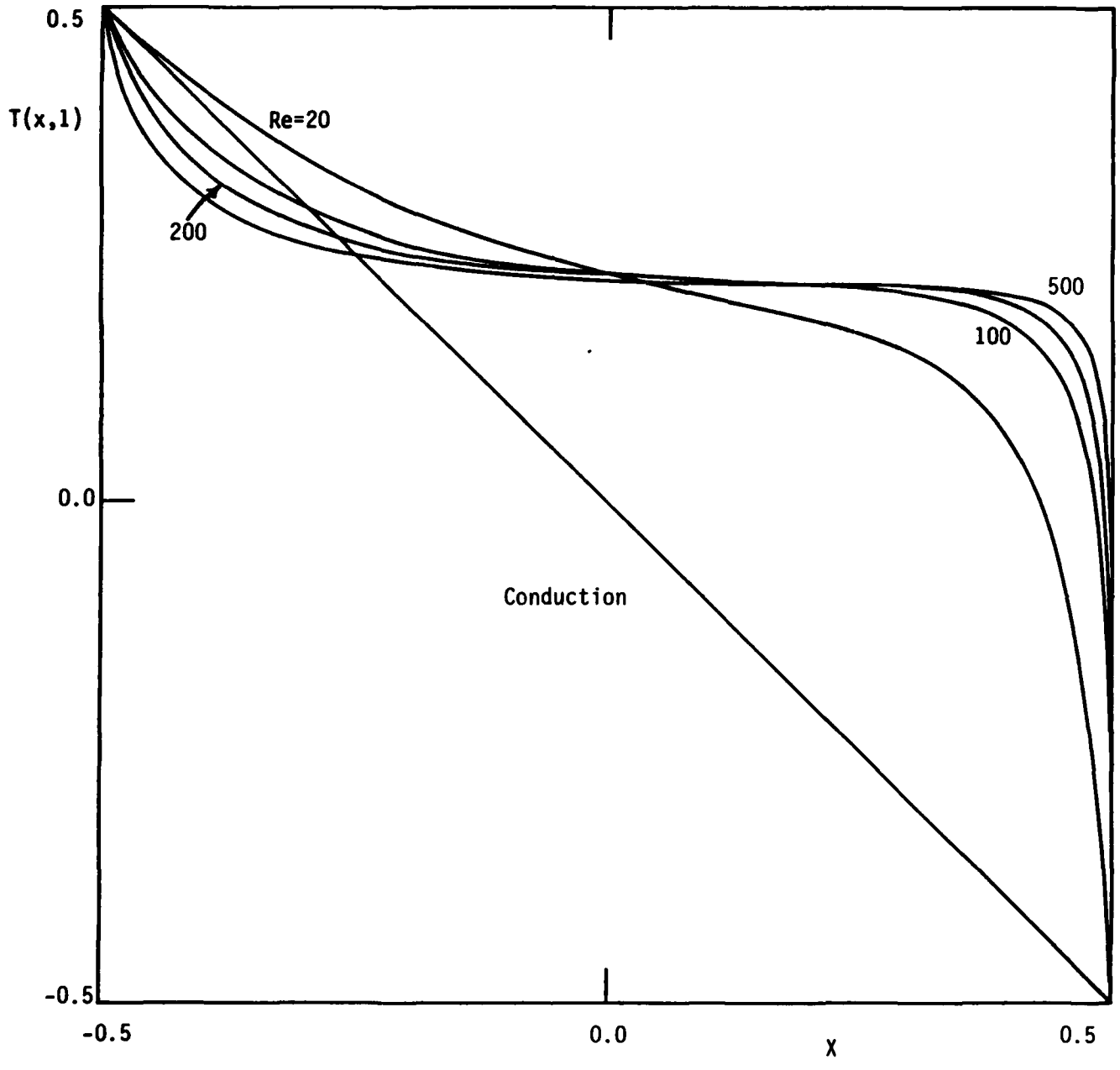

Figure 7b

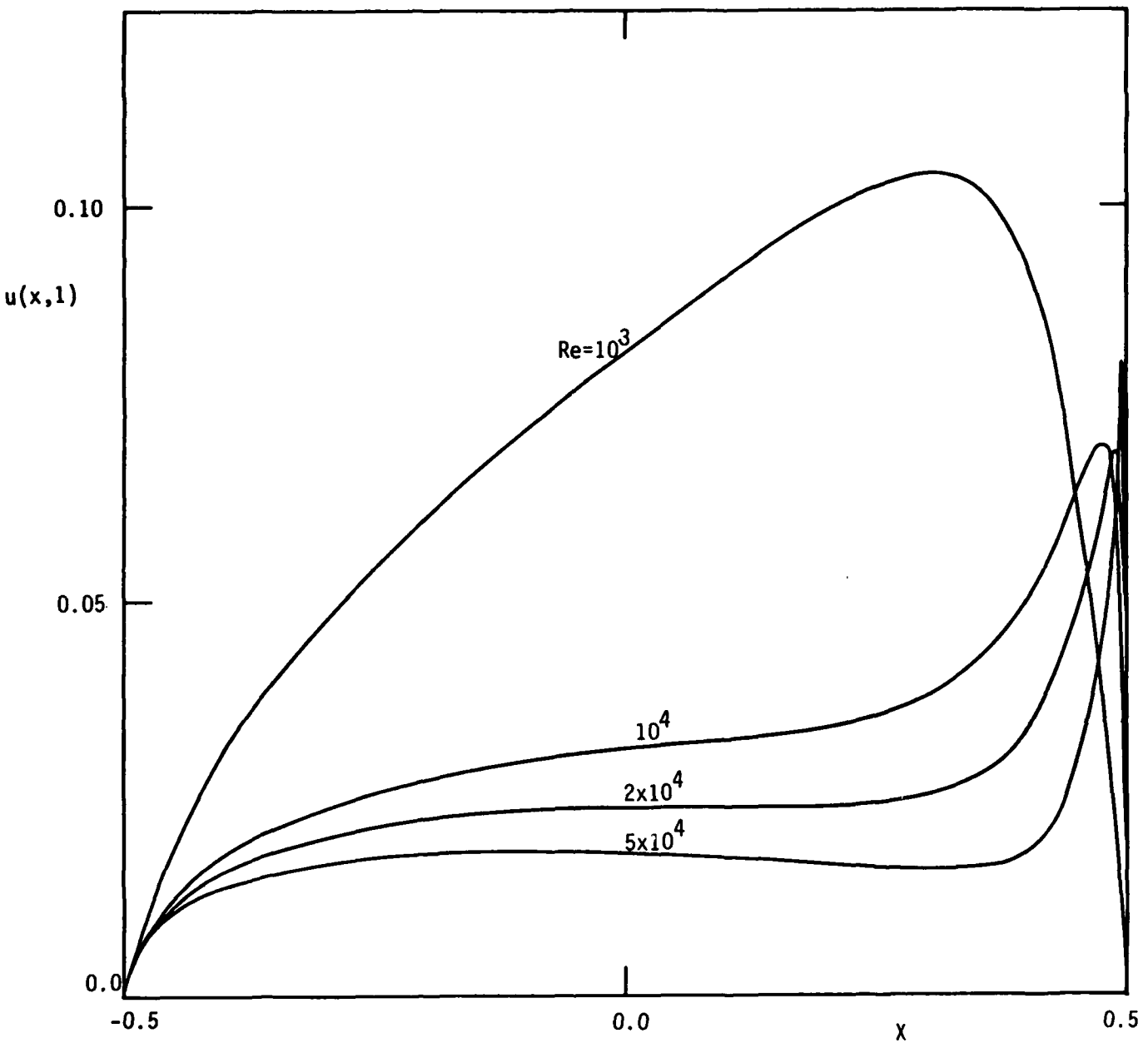

Figure 8a

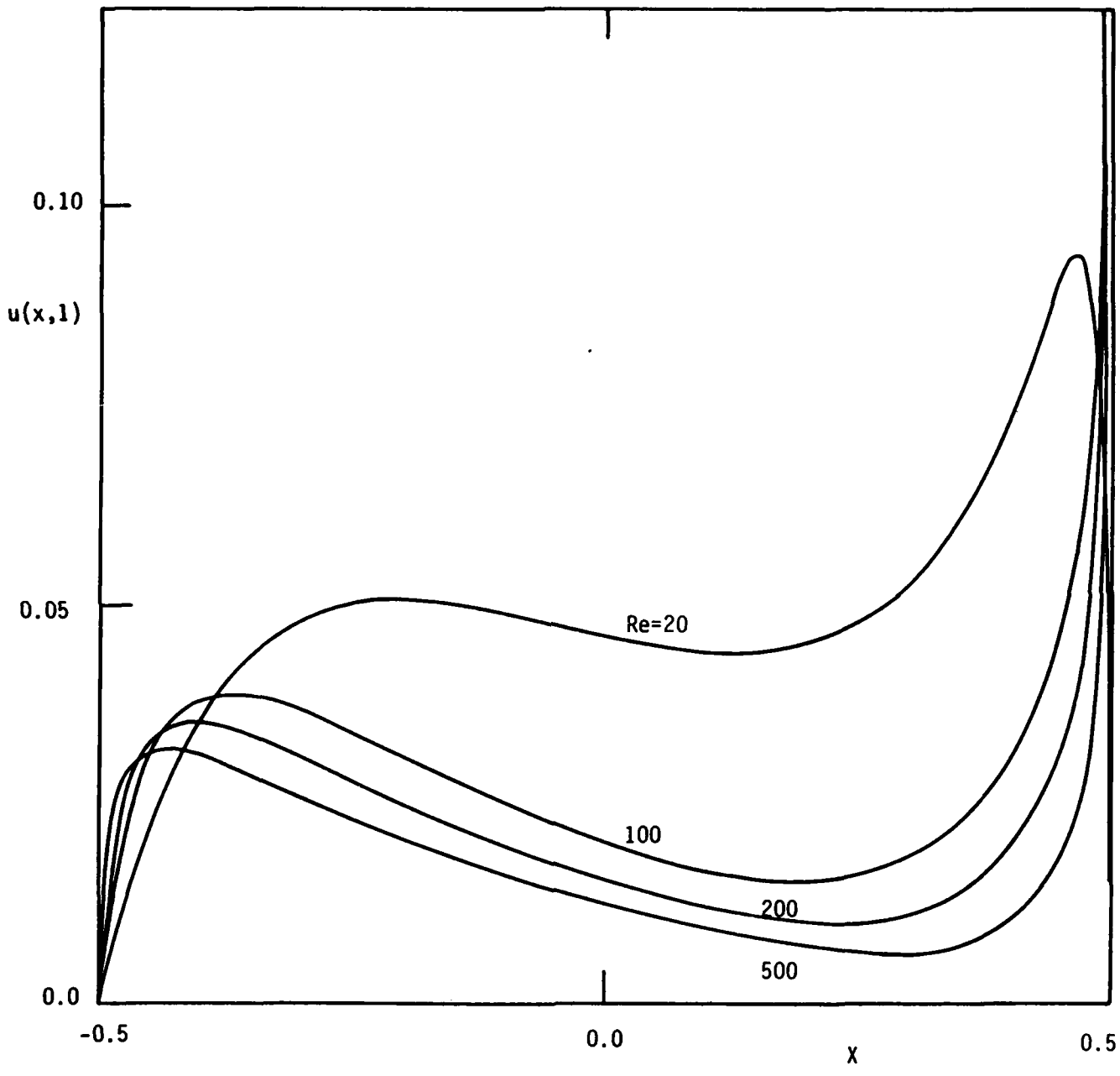

Figure 8b

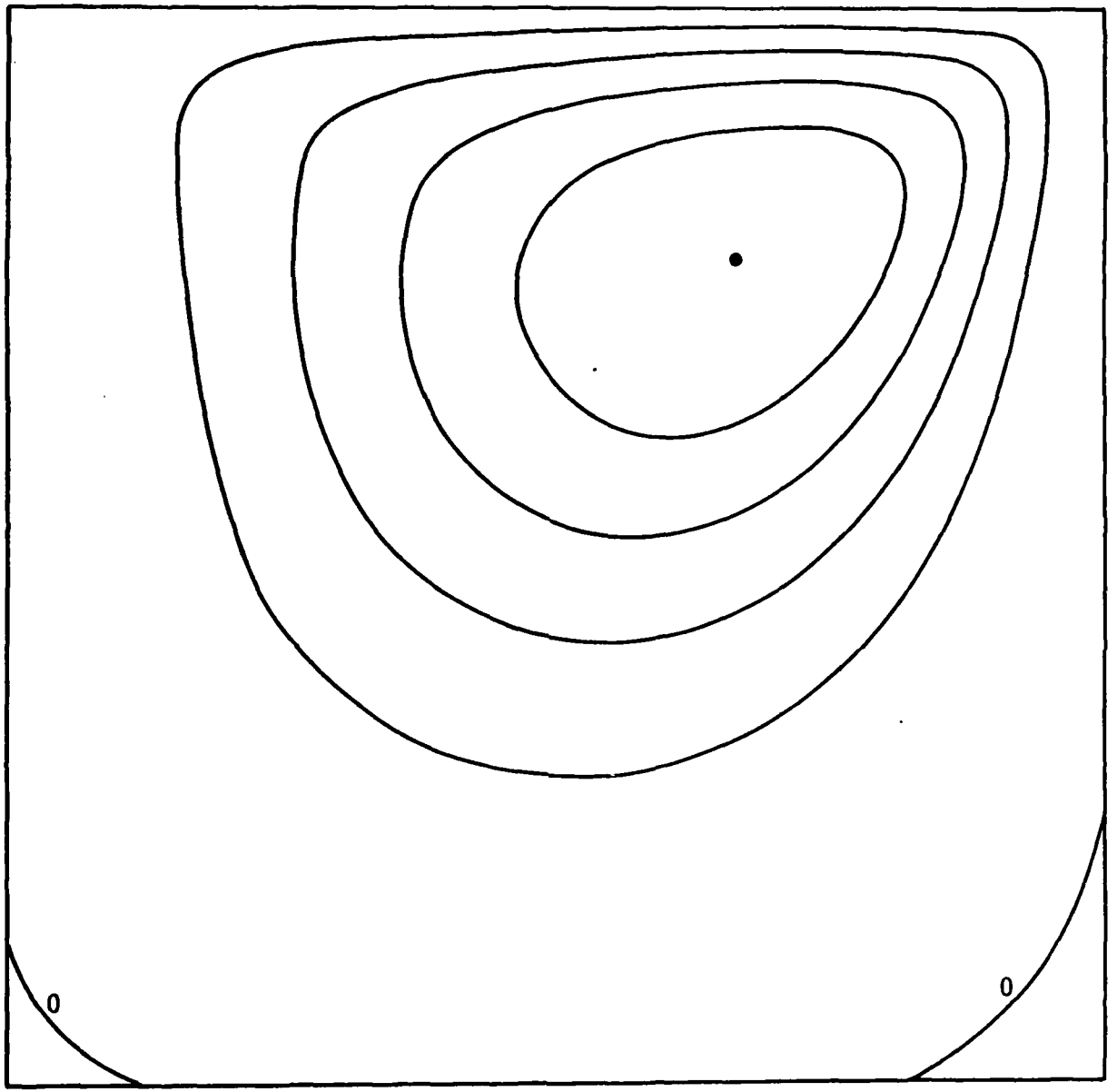

Figure 9a

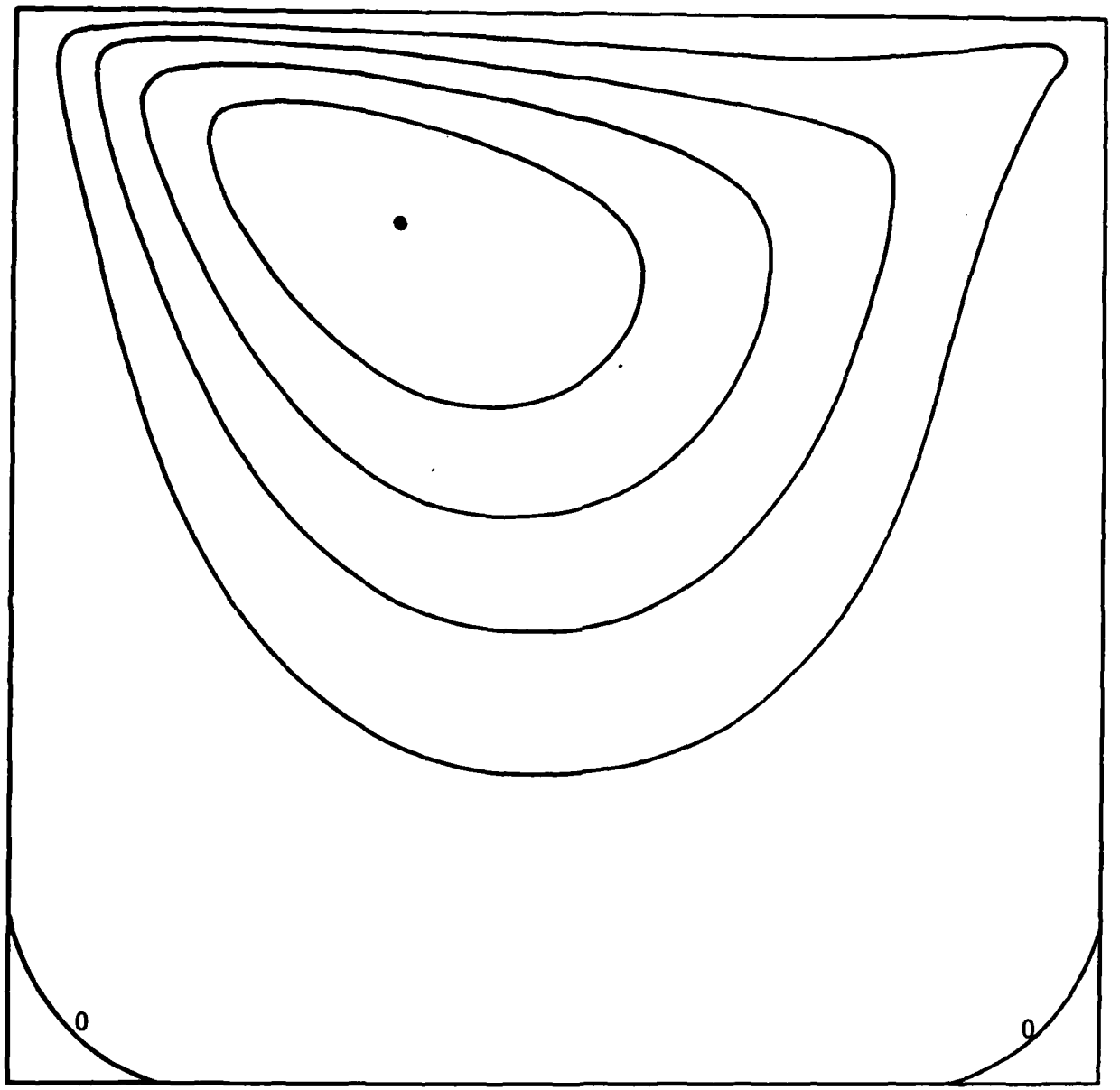

Figure 9b

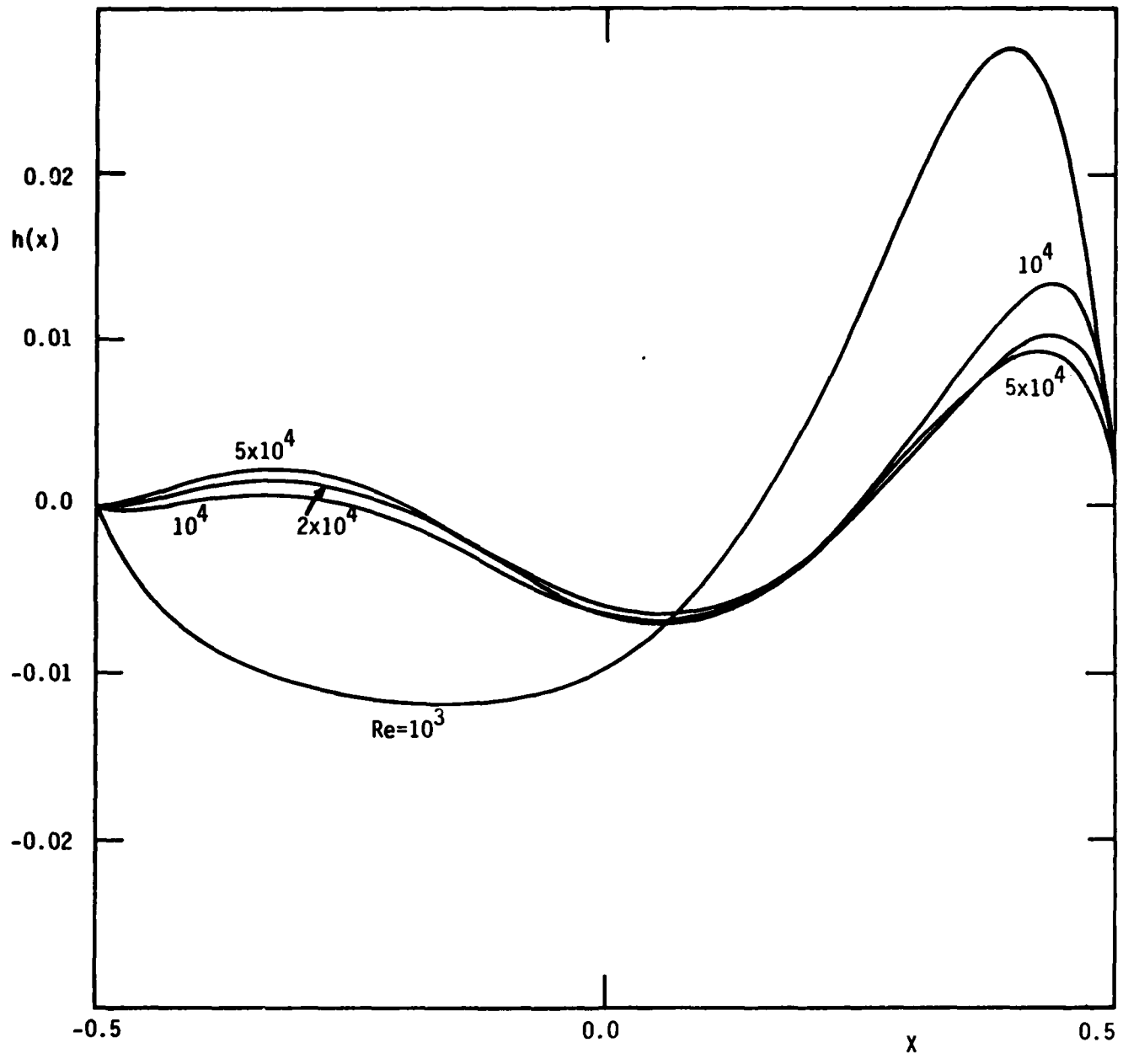

Figure 10a

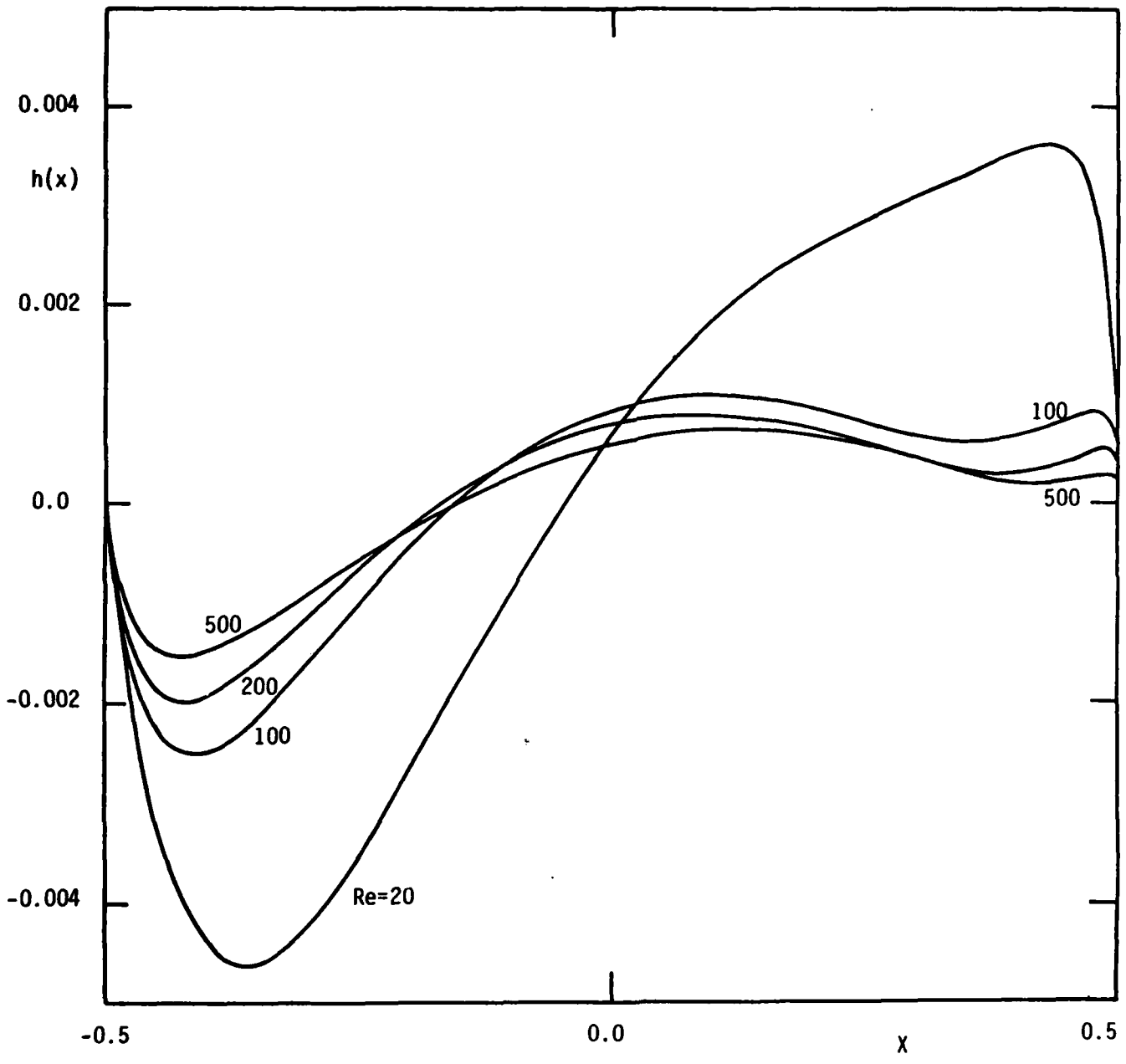

Figure 10b

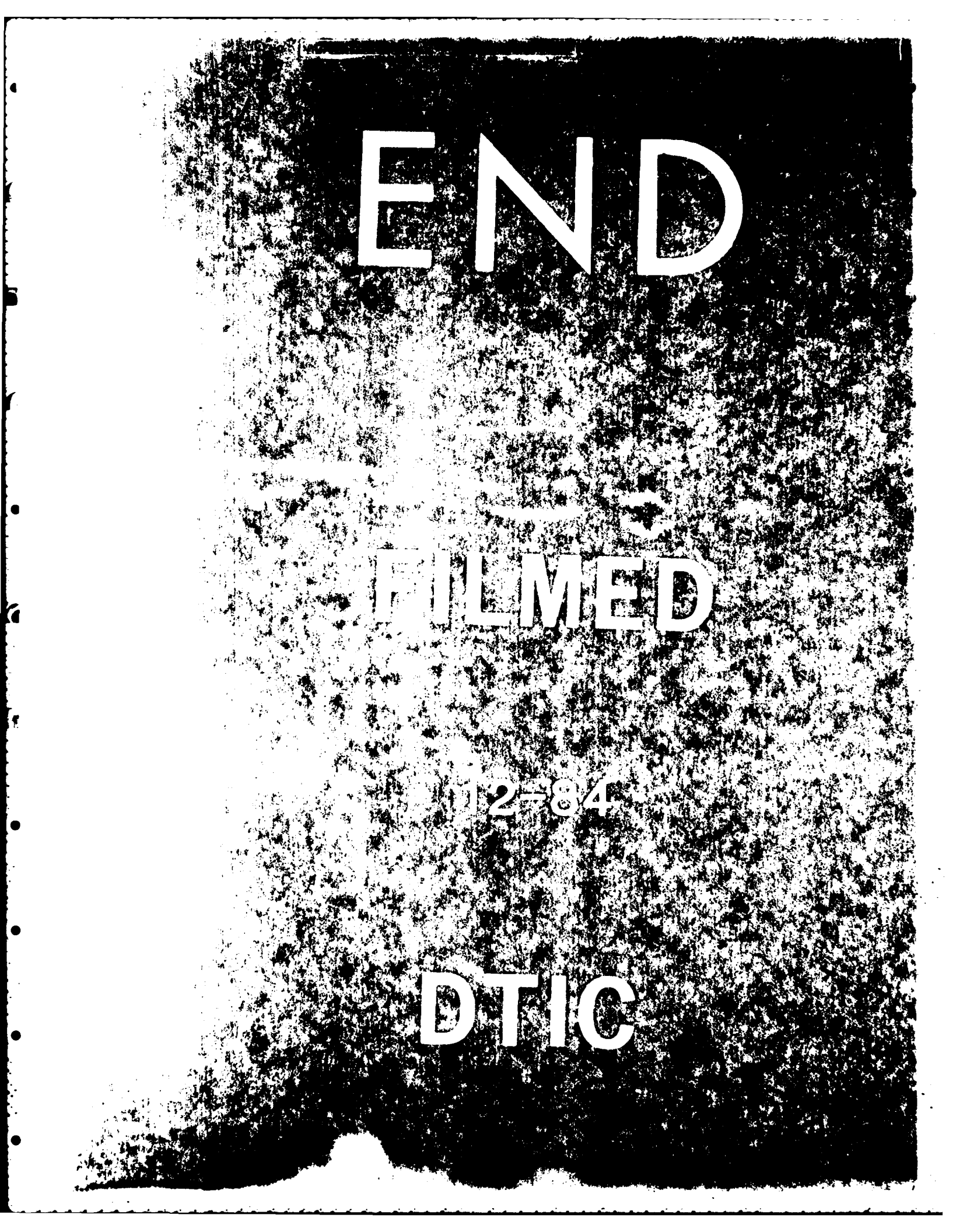
END
FILMED
12-84
DTIC